2017-11-15

Rapid fore-arc extension and detachment-mode spreading following subduction initiation

Morris, A

10.1016/j.epsl.2017.08.040
Earth and Planetary Science Letters
Elsevier BV

Morris, A., Anderson, M. W., Omer, A., Maffione, M. and van Hinsbergen, D. J. J., 2017. Rapid fore-arc extension and detachment-mode spreading following subduction initiation. *Earth and Planetary Science Letters,* **478**, 76-88, doi: 10.1016/j.epsl.2017.08.040

Rapid fore-arc extension and detachment-mode spreading following subduction initiation

Antony Morris[a*], Mark W. Anderson[a], Ahmed Omer[a,#], Marco Maffione[b], Douwe J. J. van Hinsbergen[c]

[a] *School of Geography, Earth and Environmental Sciences, University of Plymouth, Drake Circus, Plymouth PL4 8AA, UK*

[b] *School of Geography, Earth and Environmental Sciences, University of Birmingham, Edgbaston, Birmingham B15 2TT, UK*

[c] *Department of Earth Sciences, University of Utrecht, Utrecht, Netherlands*

* Corresponding author.

E-mail address: amorris@plymouth.ac.uk (A. Morris).

ABSTRACT

Most ophiolites have geochemical signatures that indicate formation by suprasubduction seafloor spreading above newly initiated subduction zones, and hence they record fore-arc processes operating following subduction initiation. They are frequently underlain by a metamorphic sole formed at the top of the downgoing plate and accreted below the overlying suprasubduction zone lithosphere

[#] Permanent address: Technical Institute of Kirkuk, Kirkuk, Republic of Iraq

immediately following ophiolite formation. Paleomagnetic analyses of ophiolites can provide important insights into the enigmatic geodynamic processes operating in this setting via identification of tectonic rotations related to upper plate extension. Here we present net tectonic rotation results from the Late Cretaceous Mersin ophiolite of southern Turkey that document rapid and progressive rotation of ophiolitic rocks and their associated metamorphic sole. Specifically, we demonstrate that lower crustal cumulate rocks and early dykes intruded into the underlying mantle section have undergone extreme rotation around ridge-parallel, shallowly-plunging axes, consistent with oceanic detachment faulting during spreading. Importantly, later dykes cutting the metamorphic sole experienced rotation around the same axis but with a lower magnitude. We show that these rotations occurred via a common mechanism in a pre-obduction, fore-arc setting, and are best explained by combining (hyper)extension resulting from detachment-mode, amagmatic suprasubduction zone spreading in a fore-arc environment with a recently proposed mechanism for exhumation of metamorphic soles driven by upper plate extension. Available age constraints demonstrate that extreme rotation of these units was accommodated rapidly by these processes over a time period of < ~3 Myr, comparable with rates of rotation seen in oceanic core complexes in the modern oceans.

Keywords: ophiolite; paleomagnetism; subduction initiation; suprasubduction zone; fore-arc extension; metamorphic sole

1. Introduction

Ophiolites provide insights into fundamental oceanic tectonic processes associated with their formation at spreading axes and subsequent intraoceanic- and emplacement-related deformation. The majority of the world's ophiolites have a geochemical signature interpreted as indicating formation above newly initiated intraoceanic subduction zones, in so-called suprasubduction zone environments (e.g. Pearce and Robinson, 2010). This setting can also account for the observation that ophiolite accretion is often closely followed by subduction-related emplacement onto continental margins (Robertson 2002). In contrast to true mid-ocean ridge systems, suprasubduction zone ophiolite formation and subsequent evolution is the result of a complex process controlled by both the subducting plate and tectonic processes in the fore-arc region. This is clearly demonstrated by the occurrence of so-called metamorphic soles below many suprasubduction zone ophiolites. Metamorphic soles are thin (< 500 m) layers of granulite to greenschist facies rocks, which experienced high temperature and pressure metamorphism (850-900°C, 10-15 kbar) above a subducting lithosphere, prior to their accretion to the overriding plate (for a review see van Hinsbergen *et al.,* 2015). In several well-preserved ophiolites like that of Oman, the metamorphic sole is spread over a broad area below the ophiolite, up to c. 100 km away from the paleo-trench, suggesting original accretion as a large semi-continuous metamorphic layer. The accretion of metamorphic soles below ophiolites necessarily requires some sort of fore-arc thinning to exhume the sole from peak metamorphic depths, either tectonically via extension of the overriding plate (e.g. Hacker and Gnos, 1997), or magmatically via partial melting and resulting volume decrease of the forearc mantle wedge below the newly formed suprasubduction zone

crust (van Hinsbergen *et al.,* 2015). The similarity of ages of ophiolitic crust and peak metamorphism of associated metamorphic soles observed in nearly all ophiolites indicates that spreading and metamorphic sole exhumation are almost simultaneous processes, and both occur during or shortly after subduction initiation.

Obtaining geological evidence that constrains the kinematics and timing of tectonic processes affecting fore-arc systems during subduction initiation in the modern oceans is difficult as incipient subduction zones are rare (Gurnis et al., 2004). Hence, well-exposed ophiolites provide important records of fore-arc processes operating during and following subduction initiation that are otherwise difficult to investigate (Stern and Bloomer, 1992; Robertson 2002). Numerous studies have highlighted how paleomagnetic analyses of ophiolites can help to unravel the tectonic evolution of these systems. A focus has been the Tethyan ophiolites of the eastern Mediterreanean/Middle East region, where magnetic techniques have been used to constrain the structure and orientation of suprasubduction spreading axes (e.g. Allerton and Vine, 1987; Hurst *et al.,* 1992; Morris and Maffione, 2016; Maffione *et al.,* 2017), patterns of magmatic flow during crustal accretion (e.g. Staudigel *et al.,* 1992; Granot *et al.,* 2011), the kinematics of transform fault systems (e.g. Morris *et al.,* 1990; MacLeod *et al.,* 1990; Morris and Maffione, 2016), and the response of the upper plate to impingement of continental margins with subduction zones (Clube *et al.,* 1985; Inwood *et al.,* 2009; Morris *et al.,* 2002).

Renewed interest in ophiolites has followed the discovery of the importance of oceanic detachment faulting and the formation of oceanic core complexes (OCCs) in slow-ultraslow spreading lithosphere in the Atlantic and Indian Oceans (e.g. Smith *et*

al., 2008; MacLeod *et al.,* 2017) and the definition of a new amagmatic "detachment-mode" of seafloor spreading (Escartín and Canales 2011). This is fundamentally different from classic magmatic spreading and involves plate divergence being taken up by slip on lithospheric-scale faults that rotate during displacement, resulting in exhumation of their footwall sections and exposure of lower crustal and mantle rocks on the seafloor. Studies of samples recovered by scientific ocean drilling have shown 45-65° rolling-hinge rotations of OCC footwalls in the Atlantic Ocean around ridge-parallel, sub-horizontal axes (Garcés and Gee, 2007; Morris *et al.,* 2009; MacLeod *et al.,* 2011). This characteristic has allowed Maffione et al. (2013) to extend the record of detachment-mode spreading back to the Jurassic by demonstrating the existence of a fossil OCC preserved within the Mirdita ophiolite of Albania. More recently, Maffione et al. (2015) showed that oceanic detachment faulting was responsible for large tectonic rotations and extensional thinning of fore-arc lithosphere preserved in the Cretaceous ophiolites of southern Tibet. This led them to propose a new concept of "fore-arc hyperextension", demonstrating how the exchange of ideas between studies in the modern oceans and in ophiolites can lead to advances in our understanding of lithospheric processes.

Here we present the first paleomagnetic data from the Late Cretaceous Mersin ophiolite of southern Turkey. Like many Tauride ophiolites (Dilek *et al.,* 1999), Mersin consists predominantly of tectonized mantle rocks and ultramafic/mafic cumulates, with no sheeted dyke complex and only limited exposures of extrusive rocks, and is underlain by a metamorphic sole that has ^{40}Ar-^{39}Ar cooling ages that are similar to the age of the ophiolitic magmatic rocks (Parlak *et al.,* 2013; van Hinsbergen *et al.,* 2016). Our data constrain the axes, magnitudes and timing of tectonic rotations in

124 these units, and provide evidence for rapid fore-arc (hyper)extension via detachment-
125 mode seafloor spreading (Escartin and Canales*,* 2011). We show that this style of
126 Neotethyan suprasubduction zone spreading provides a viable mechanism to explain
127 the exhumation of metamorphic soles, their structural disruption following welding to
128 the base of the lithosphere, and the lack of upper crustal sequences in many Tauride
129 ophiolites.
130
131 **2. The Mersin ophiolite**
132
133 The Mersin ophiolite complex outcrops over a 60 km long, 25 km wide area in
134 southern Turkey (Fig. 1a). It consists of an Upper Cretaceous ophiolite sequence,
135 underlain by metamorphic sole rocks and then by the Mersin Mélange (Fig. 1b;
136 Parlak and Delaloye, 1996, 1999; Parlak *et al.,* 2013). These units form the highest
137 structural unit of the uppermost Cretaceous-Eocene Tauride fold-thrust belt
138 dominated by Paleozoic-Mesozoic platform carbonates (Robertson, 2002).
139
140 The ophiolite has a suprasubduction zone geochemical signature (Parlak *et al.,*
141 1996a) and consists of tectonized peridotites (harzburgites and dunites), ultramafic
142 and mafic cumulates, isotropic gabbro, minor plagiogranites, and rare basalts
143 associated with deep marine sediments (Parlak *et al.,* 1996a). The cumulate rocks
144 are best exposed along the Sorgun valley (between the villages of Sorgun and
145 Arsalanlı; Fig. 1a), where ~800 m of ultramafic cumulates at the base pass upwards
146 into ~2500 m of modally layered gabbroic rocks consisting of gabbro, olivine gabbro
147 and anorthosite (Parlak *et al.,* 1996a). Way-up criteria (mineralogical grading;
148 evidence of scouring at the base of some layers; Fig. 2) indicate that steeply-dipping

149 modal compositional layering in the gabbros is in places overturned. The cumulate
150 layers are occasionally intruded at a high angle by thin, fine-grained basaltic dykes.
151
152 Lower levels of the ophiolite are best exposed in the Fındıkpınarı valley area (Fig.
153 1a), nearly 20 km to the NE of the Sorgun valley, providing sections through both the
154 mantle sequence and the metamorphic sole. The latter has a thickness of about 50-
155 70 m and consists predominantly of amphibolites, amphibolitic schists, epidote-
156 amphibolite schists, quartz-mica schists, calcschists and marble, with a typical
157 inverted metamorphic zonation from upper amphibolite at the top to greenschist
158 facies at the bottom (Parlak *et al.,* 1996b). The sole rocks are intensely deformed,
159 with development of a pronounced foliation, a NW-SE-trending mineral stretching
160 lineation and intrafolial folds (Parlak *et al.,* 1996b). Kinematic indicators all indicate a
161 top to the NW shear sense during formation of the sole (Parlak *et al.,* 1996b).
162
163 Both the tectonized harzburgite and sole are cut by undeformed, discrete doleritic
164 dykes composed of plagioclase, clinopyroxene and amphibole, with subophitic and
165 microgranular textures and variable degrees of hydrothermal alteration. They have
166 geochemical signatures similar to evolved island-arc tholeiites and were derived from
167 a mantle wedge that underwent previous melt extraction and subsequent
168 metasomatism by LILE- and light REE-enriched fluids (Dilek *et al.,* 1999). Dykes
169 hosted by tectonized harzburgite are up to 5 m thick and dip at ~30° to the ~ESE,
170 whereas those hosted by the metamorphic sole are characteristically thinner (< 1 m),
171 clearly post-metamorphic and post-shearing, and dip at ~55° to the ~NW.
172

Available high precision ^{40}Ar–^{39}Ar and U-Pb age constraints for the Mersin ophiolite and its metamorphic sole are summarized in Table 1. Only one U-Pb zircon date is available from the Mersin gabbros (Parlak et al., 2013), yielding an age of 82.8±4.0 Ma. This Is deemed unreliable, however, due to evidence for hydrothermal alteration of the dated zircons, and the age of crystallization of the suprasubduction zone crust regionally is considered by Parlak et al. (2013) to be ~89 Ma. The remaining data indicate that intrusion of dykes into the mantle sequence, formation of the metamorphic sole (cooling through amphibolite facies conditions) and intrusion of dykes through the sole were broadly synchronous events. This has important implications for the rapidity of the rotations determined from the paleomagnetic data presented here.

3. Sampling and methods

To quantify tectonic rotations that have affected the Mersin ophiolite, we sampled the lower crustal sequence (ultramafic and gabbroic cumulates) exposed continuously along the Sorgun valley section (Fig. 1a), together with dolerite dykes cutting tectonized harzburgites of the mantle sequence, and dolerite dykes cutting the metamorphic sole of the ophiolite (both exposed near the village of Fındıkpınarı; Fig 1a). An average of eight samples per site were drilled *in situ* using standard paleomagnetic procedures, yielding up to 13 specimens per site for analysis. Sampling was restricted to exposures that showed either consistent planar layering in cumulate rocks or dykes with parallel planar margins. Structural orientations were measured in the field to an accuracy of ± 5°.

198 Natural remanences were measured in the University of Plymouth palaeomagnetic
199 laboratory using either Molspin or AGICO JR-6A fluxgate spinner magnetometers
200 (with respective noise levels of 0.05 x 10^{-3} and 0.01 x 10^{-3} A/m). Specimens were
201 subjected to either alternating field (AF) demagnetization using an AGICO LDA-3A
202 demagnetizer in 13 incremental steps from 5 to 100 mT or thermal demagnetization
203 using a Magnetic Measurements MMTD80A demagnetizer with 19 temperature
204 increments from 100 to 580°C (or until complete demagnetization). Demagnetization
205 data were displayed on orthogonal vector plots and remanence components isolated
206 via principal component analysis using MacPaleomag software (written by Jeff Gee,
207 Scripps Institution of Oceanography). Site mean directions were evaluated using
208 Fisherian statistics on virtual geomagnetic poles (VGPs) corresponding to the
209 isolated characteristic remanent magnetizations (ChRMs). Paleomagnetic quality
210 criteria proposed by Deenen et al. (2011) were adopted to estimate the reliability of
211 the ChRM/VGP distribution at the site level. In particular, the VGP scatter (i.e., A_{95})
212 obtained at each site was compared to the expected scatter induced by paleosecular
213 variation (PSV) of the geomagnetic field (i.e., A_{95min} - A_{95max}) to assess whether PSV
214 was sufficiently represented in our datasets (Deenen *et al.,* 2011). For values of A_{95} <
215 A_{95min} PSV is not adequately represented, indicating insufficient time averaging of the
216 geomagnetic field (i.e. resulting from rapid cooling), slow cooling and protracted
217 acquisition of remanence (such that PSV is largely averaged at the specimen level)
218 or remagnetization. Conversely, values of A_{95} > A_{95max} may indicate additional
219 (tectonic) processes responsible for an enhanced scatter of paleomagnetic
220 directions. Site mean magnetization directions were interpreted using a net tectonic
221 rotation approach (Allerton and Vine, 1987; Morris *et al.,* 1998) to determine rotation

axes and magnitudes and recover the initial strikes of dykes. This technique is discussed more fully below.

Rock magnetic experiments were performed to characterize remanence-carrying minerals in sampled lithologies. The high-temperature (20-700°C) variation of magnetic susceptibility, *k*, of representative samples was measured in an argon atmosphere using an AGICO Kappabridge KLY-3S coupled with a CS-3 furnace. Curie temperatures were determined from these experiments by the Petrovsky & Kapička (2006) method on 1/*k* data using the AGICO program Cureval v. 8.0.2. Isothermal remanent magnetization (IRM) acquisition experiments were conducted on representative samples to determine coercivity spectra (using a Molspin pulse magnetizer to apply peak fields up to 800 mT, with resulting IRMs measured using an AGICO JR-6A spinner magnetometer), followed by backfield IRM experiments to determine coercivities of remanence. Ferromagnetic phases were further characterized in thin section by optical microscopy and by EDX spectral analyses performed on a JEOL7001 FEG-SEM and analyzed using Oxford Instruments Aztec software.

4. Results and analysis

4.1 Magnetic mineralogy and palaeomagnetic results from the ophiolite

High-temperature variation of magnetic susceptibility experiments revealed consistent maximum Curie temperatures of ~580°C (Figure 3a), indicating that the ferromagnetic fraction in both cumulate rocks and dykes includes near-stoichiometric

magnetite. Some specimens exhibit increased susceptibility upon cooling, suggesting production of new magnetite during heating. A limited number of specimens (e.g. specimen MC1804 in Fig. 3a) show a hump in the heating curve between 150-400°C. The increasing temperature limbs of these humps are reversible until 300°C, but become irreversible after further heating, suggesting the presence of titanomagnetite/titanomaghemite in addition to magnetite. IRM acquisition experiments show that saturation is reached at applied fields of 200-300 mT (Figure 3b) indicating presence of low coercivity minerals in these rocks. Backfield IRM experiments yield coercivity of remanence values of 24-53 mT suggesting presence of fine-grained single domain or pseudo-single domain magnetite. These rock magnetic observations are consistent with petrographic and SEM analyses that show that magnetite and minor titanomagnetite are the dominant oxides present in both cumulate rocks and dykes. In the ultramafic cumulates (sites MC01-03), secondary magnetite is present in serpentinized olivine grains, whereas primary magnetite (plus titanomagnetite) with little alteration is observed in the cumulate gabbros and diabase dykes. Ferromagnetic pyrrhotite is also occasionally seen in the dykes, but demonstrably carries the same magnetization direction as the dominant magnetite phase. Overall, these results are entirely compatible with those obtained in other Late Cretaceous Neotethyan ophiolites in this region (e.g. Troodos, Hatay, Baër-Bassit, Alihoca, Göksun, Divriği; Morris *et al.,* 1998, 2002; Inwood *et al.,* 2009; Morris and Maffione, 2016; Maffione *et al.,* 2017), where magnetic remanences have been shown to be of primary, pre-deformational origin, acquired during or shortly after seafloor spreading.

Intensities of natural remanences in these rocks vary by lithology, with highest average intensities in the layered gabbros (1.12 A/m) and lower values of 132 mA/m and 80 mA/m in the ultramafic cumulates and dykes, respectively. Stable components of magnetization were isolated at all sites, following removal of occasional minor secondary components during initial demagnetization. Typical examples of demagnetization behaviour are shown in Fig. 4. Most samples are dominated by univectorial, single component decay to the origin. Both AF and thermal demagnetization experiments yielded identical remanence directions (Fig. 4). Stable components of magnetization were identified from individual specimens and subsequently combined to give a mean ChRM for each site. These *in situ* magnetic remanences are given in Table 2 and shown with corresponding specimen directions and VGPs in the stereographic equal area projections of Supplemental Fig. 1. With the exception of one specimen (at site MD11), all VGPs fell within the 45° cut-off at each site recommended by Johnson et al. (2008). Directions are unrelated to the present-day geocentric axial dipole field in the Mersin region (D = 000°, I = 56°), excluding recent remagnetization. Cumulate rocks (ultramafic cumulates and layered gabbros) have NE-directed *in situ* ChRMs with negative inclinations, indicating substantial tectonic rotation since magnetization acquisition. Dykes hosted in the mantle sequence also have *in situ* negative inclinations, whereas those cutting the metamorphic sole have shallow positive inclinations, with both sets having generally northerly declinations.

VGP scatter at 11 out of 28 sites (Table 2) is within the limits of that expected from PSV (Deenen *et al.,* 2011), consistent with a primary origin of the remanence. Underrepresentation of PSV at remaining sites is interpreted to reflect significant

296 averaging of secular variation at the sample level during slow cooling of the cumulate
297 rocks (as seen in samples of lower crustal gabbros recovered by scientific ocean
298 drilling; Gee and Kent, 2007) and of dykes intruded into the mantle sequence and
299 metamorphic sole.
300
301 *4.2 Reference direction*
302
303 Remanence directions must be compared to an appropriate reference direction to
304 determine the extent of tectonic rotation affecting the ophiolite. In our analysis, the
305 reference direction has a declination = 000°, assuming an original normal magnetic
306 polarity as the ophiolite formed during the Cretaceous Normal Superchron (C34N).
307 This implies that calculated net rotations arise from a combination of plate motion
308 and intra-plate deformation. The inclination of the reference direction was determined
309 from paleolatitude estimates based on kinematic reconstructions (van Hinsbergen *et*
310 *al.,* 2016) placed in the paleomagnetic reference frame of Torsvik et al. (2012).
311 Uncertainties in the reference inclination relate to the reconstructed width of the
312 Neotethys Ocean and the A_{95} error of the reference global apparent polar wander
313 path. Reconstructions for the Late Cretaceous at 100-90 Ma constrain the
314 Neotethyan spreading axis to lie between the southern margin of Eurasia at 33±3°N
315 and the northern margin of Gondwana at 16±3°N. We have no other paleolatitudinal
316 control on the position of the future Mersin ophiolite within these limits, and therefore
317 used a paleolatitude of 24.5±11.5°N to encompass this range. Assuming a geocentric
318 axial dipole field, this corresponds to a reference inclination of 40.2±15.4°.
319
320 *4.3 Determination of net tectonic rotations*

Standard paleomagnetic structural corrections involve untilting inferred paleohorizontal/vertical surfaces around strike-parallel axes. Corrected declinations are then compared to the reference direction to determine vertical axis rotations. This approach therefore arbitrarily decomposes the total deformation at a site into rotations around two orthogonal axes (vertical and horizontal). Interpretations then frequently focus entirely on the vertical axis rotations, ignoring the tilting component of the deformation. In complexly deformed terrains, where fold axes are seldom horizontal and where multiple phases of deformation may occur, this procedure can introduce serious declination errors (MacDonald, 1980). It is more appropriate, therefore, to describe the deformation at a site in terms of a single rotation about an inclined axis, which restores both the paleosurface to its initial orientation and the site mean magnetization vector to the reference direction. This single rotation may then be decomposed into any number of component rotations on the basis of additional structural data. Importantly, in the case of dykes, this approach can resolve rotations around margin-normal axes that are impossible to observe in the field and that act as a source of error when standard tilt corrections are employed (Morris and Anderson, 2002). This approach also facilitates back-stripping of later rotations from the total deformation to recover earlier rotations.

Here we use the net tectonic rotation method of Allerton and Vine (1987), which has been employed effectively in numerous previous studies in ophiolites (e.g., Morris *et al.,* 1990, 1998, 2002; Hurst *et al.,* 1992; Inwood *et al.,* 2009; Maffione et al, 2015, 2017; Morris and Maffione, 2016, van Hinsbergen *et al.,* 2016). This technique (Supplemental Fig. 2) can be applied to either paleovertical or paleohorizontal cases,

346 with the key assumption that no internal deformation of a sampled unit has occurred.
347 In this case, the angle β between the site magnetization vector (SMV) and the
348 present day pole to the paleosurface (PDP) remains constant during deformation
349 (Allerton and Vine, 1987). A circle of radius β centred on the reference magnetization
350 vector (RMV) therefore defines the locus of potential positions of the initial pole to the
351 paleosurface. In the case of a dyke, the intersections of this circle with the horizontal
352 represent the poles to two possible vertical initial dyke orientations (Supplemental
353 Fig. 2), and additional constraints are required to select a preferred solution. If a
354 vertical solution cannot be found then the dyke initial strike is invariable and fixed by
355 the reference direction and we exclude the result from the analysis of restored dyke
356 trends. In the case of cumulate rocks, an initial pole for the paleosurface is selected
357 at the steepest point on the circle of radius β centred on the RMV in order to restore
358 the structure to a minimum possible dip (Supplemental Fig. 2). In all cases, the SMV
359 is then restored to the RMV and the PDP to its initial orientation by rotating around an
360 axis at the intersection of the planes (great circles) bisecting the pairs of vectors
361 (Supplemental Fig. 2). The net tectonic rotation is described by the azimuth and
362 plunge of this rotation axis and the angle and sense of rotation.
363
364 In a modification of this method used here (Morris *et al.,* 1998; Koymans *et al.,* 2016),
365 the effects of uncertainties on the input vectors are modelled by applying the Allerton
366 and Vine (1987) algorithm to all combinations of three estimates of the reference
367 inclination (mean plus two values at the edge of its error bar), and five estimates
368 each of the SMV and present day pole to paleosurface (see Supplemental Fig. 2).
369 This yields 75 estimates of the rotation parameters at each site, defining a non-
370 circular distribution of acceptable rotation axes. The mean rotation axis can be

371 determined using Bingham statistics (orientation of maximum eigenvector), and the
372 distribution of rotation angles plotted as histograms (Supplemental Fig. 2) and
373 described by the mean value and standard deviation. Restored dyke trends can be
374 represented on rose diagrams, with the mean strike determined from the
375 intermediate eigenvector of the corresponding distribution of initial dyke poles. When
376 distributions of rotation parameters at multiple sites overlap, these may be
377 amalgamated to determine the most robust overall solution.
378
379 *4.4 Net tectonic rotation solutions*
380
381 Out of 28 sampled sites, 25 gave net tectonic rotation solutions that are considered
382 reliable. The three rejected sites are: (i) two dyke sites (MD01 and MD10) that gave
383 scattered rotation axes and too few vertical solutions to be considered reliable; and
384 (ii) a thin basaltic dyke (site MC10) intruding the layered gabbros of site MC09, that
385 has a direction of magnetization statistically indistinguishable from its host rocks and
386 that is not considered separately in the analysis of rotations. Mean net tectonic
387 rotation parameters at the remaining sites are given in Table 3. In the case of the
388 dyke sites (Table 3), our preferred solutions are those with NE-SW-directed rotation
389 axes as these: (i) are consistent with results from the cumulate section; (ii) yield more
390 consistent rotation angles between sites than the alternative solutions; and (iii)
391 produce initial NE-SW dyke strikes that are in agreement with a regional-scale
392 dataset of restored Neotethyan paleo-spreading directions recently reported by
393 Maffione et al. (2017).
394

Fig. 5 illustrates the distributions of rotation parameters amalgamated by lithostratigraphic level in the ophiolite, whereas results at individual sites are shown in Supplemental Fig. 3 (for dyke sites) and Supplemental Fig. 4 (for cumulate sites). The analyses demonstrate that all levels of the Mersin ophiolite have experienced significant tectonic rotation around shallowly-plunging, NE-SW-directed axes. The overall mean rotation parameters (Tables 3 and 4; Fig. 5) for the three sampled lithostratigraphic levels are:

Cumulate section: 120.0°±27.4° clockwise rotation, axis = 058°/23°, N = 1200
Mantle-hosted dykes: 125.0°±8.4° clockwise rotation, axis = 047°/-04°, N = 257
Metamorphic sole-hosted dykes: 45.0°±11.8° clockwise rotation, axis = 040°/31°, N = 290

where errors on rotation angles are ± 1 standard deviation.

This indicates that, despite a present day geographic separation of c. 20 km, the mantle and crustal sections of the ophiolite display structural integrity and experienced a common rotation history since acquiring their magnetizations. The metamorphic sole has also experienced rotation around a similar NE-SW-directed axis but with a much lower magnitude. This is considered to represent the latest phase of rotation to affect the ophiolite and potentially reflects a combination of intraoceanic and emplacement-related deformation. We assume that this net rotation also affected the overlying mantle and crustal sites. This assumption is supported by similar initial strikes for the mantle- and metamorphic sole-hosted dykes (Fig. 5), that suggests intrusion of these units occurred in a common stress field associated with

upper plate extension during formation of the ophiolite in a suprasubduction zone setting. The earlier phase of rotation affecting the mantle and crustal sections can then be determined by back-stripping the effect of the later rotation of the metamorphic sole prior to calculation of revised net tectonic rotation parameters for these units (Tables 3 and 4). This yields the following mean rotation parameters:

Cumulate section	79.9°±25.7° clockwise rotation, axis = 060°/12°, N = 1200
Mantle-hosted dykes:	92.4°±8.2° clockwise rotation, axis = 032°/-15°, N = 252
Combined:	82.1°±24.1° clockwise rotation, axis 056°/08°, N = 1452

The combined result represents the best estimate for early tilting of the sampled parts of the future ophiolite prior to emplacement of dykes into its metamorphic sole, and confirms that all phases of deformation involved rotation around similar, shallow NE-directed axes. Moreover, given the close timing of crustal accretion, cooling of the metamorphic sole and dyke intrusion (Parlak and Delaloye, 1996, 1999; Dillek et al., 1999; Parlak *et al.,* 2013), these data indicate that rotations accumulated progressively within the ophiolite over a very short time interval of < ~3 Myr, requiring a tectonic environment capable of generating rapid and large rotations.

5. Discussion

5.1 Tectonic environment for extreme and rapid early rotation of the Mersin ophiolite

The early phase of rotation documented above is demonstrably of intraoceanic origin and associated with suprasubduction zone spreading of the Mersin ophiolite as it

445 occurs between two phases of dyke emplacement. In addition, rotation axes are
446 broadly aligned with the restored trends of dykes in both the mantle sequence and
447 metamorphic sole. Assuming that these are intruded perpendicular to the
448 suprasubduction zone extension direction, this indicates rotation dominated by tilting
449 around ridge-parallel axes.
450
451 In seafloor spreading systems, large rotations around shallowly plunging axes may
452 be accommodated by normal faulting during plate divergence. For example, net
453 tectonic rotation analyses in Troodos have highlighted rotations of dykes and lavas in
454 the hanging wall of listric normal faults (Allerton and Vine, 1987; Hurst *et al.,* 1992)
455 during the development of axial and off-axis graben structures by upper crustal
456 extension. These faults dip symmetrically towards graben axes and are inferred to
457 flatten at depth to sole out into detachments at the base of the upper crust (at the
458 dyke-gabbro transition; Varga and Moores, 1985), without affecting deeper levels of
459 the ophiolite. Large listric faults that dip towards the spreading axis have also been
460 observed by seismic imaging in the slow-spreading Atlantic Ocean (e.g. Salisbury
461 and Keen, 1993), but these sole out near the base of the crust. To accommodate the
462 rotations observed in the Mersin ophiolite by listric faulting during spreading would,
463 however, require faults that sole out at the base of the lithosphere (within the upper
464 mantle). In addition, even if lithospheric-scale listric faults were capable of
465 accommodating rotation of the Mersin crust and upper mantle, they would be
466 incapable of capturing rocks of the metamorphic sole at depth (i.e. near their
467 detachment level) and rotating these as well.
468

469 In contrast to downwards-convex listric faulting, displacement on upwards-convex
470 oceanic detachment faults (Escartín and Canales, 2011) provides a viable potential
471 mechanism for rotation of upper mantle, crustal and metamorphic sole rocks.
472 Investigations of oceanic core complexes in the modern oceans (Garcés and Gee,
473 2007; Morris *et al.,* 2009; MacLeod *et al.,* 2011) have shown that rolling hinge
474 rotation of detachment fault footwalls around sub-horizontal, ridge-parallel axes is a
475 characteristic signature of these lithospheric-scale structures. Within ophiolites,
476 Maffione et al. (2013) showed that such fault systems may be recognised
477 paleomagnetically using this characteristic rotation style. Most recently, Maffione et
478 al. (2015) used a net tectonic rotation approach to document rotations around sub-
479 horizontal axes of mantle-hosted intrusions in the lower Cretaceous suprasubduction
480 zone ophiolites of south Tibet. Maffione et al. (2015) suggested that these rotations
481 result from upper plate extension accommodated by widespread detachment faulting.
482 They termed this process “forearc hyperextension” and inferred that structural
483 dismemberment occurred shortly after magmatic accretion.
484
485 We propose that the early rotation documented in the Mersin ophiolite likewise is
486 related to fore-arc (hyper)extension taken up by detachment-mode suprasubduction
487 zone spreading. This is supported by four lines of argument: (i) rolling hinge rotations
488 of the footwalls of oceanic detachment faults are characterized by ridge-parallel, sub-
489 horizontal rotation axes (Garcés and Gee, 2007; Morris *et al.,* 2009; MacLeod *et al.,*
490 2011), directly comparable to the style of rotation seen in Mersin (Fig. 6); (ii) rotation
491 during the development of oceanic core complexes occurs very rapidly, as required
492 by the full Mersin dataset based upon available age constraints. For example, along
493 the Mid Atlantic Ridge, 46° of rotation of the Atlantis Massif footwall occurred in < 1.2

494 Myr (Morris *et al.,* 2009), whereas 64° of rotation of the 15°45'N oceanic complex
495 was achieved within a very narrow inferred period of activity spanning a time interval
496 between ~2.5 to 2.1 Ma (MacLeod *et al.,* 2011); (iii) oceanic detachment faults are
497 lithospheric-scale structures that in the modern oceans have demonstrably exhumed
498 mantle rocks onto the seafloor (Cannat *et al.,* 2006), and are therefore capable of
499 rotating both crustal and mantle sections of the Mersin ophiolite around the same
500 axis, in contrast to "standard" oceanic normal faults that only affect the brittle upper
501 crust; and (iv) displacement on oceanic detachment faults tectonically juxtaposes
502 rotated lower crustal and upper mantle rocks in their footwalls with unrotated upper
503 crustal lavas in hanging wall blocks (MacLeod *et al.,* 2009), providing a plausible
504 explanation for similar geological relationships in the Mersin and other Tauride
505 ophiolites (where limited exposures of extrusive rocks are in close proximity to lower
506 crustal/upper mantle rocks without an intervening sheeted dyke complex).
507
508 We note that the c. 82° early rotation seen in the Mersin ophiolite exceeds the range
509 of footwall rotations observed in single oceanic detachment fault systems such as
510 those sampled in the Atlantic Ocean (Fig. 6). However, numerical modeling of
511 detachment faulting at slow-spreading ridges (Tucholke *et al.,* 2008) suggests that
512 the active root zone of a weak, asymmetric fault should migrate with its hanging wall
513 across the axis of rifting if magmatic accretion in the hanging wall takes up <<50% of
514 the plate separation (Tucholke *et al.,* 2008; MacLeod *et al.,* 2009; Supplemental Fig.
515 5). Reston and McDermott (2011) suggested that such migration would result in fault
516 abandonment as a new fault cuts up from the rift axis through the preceding footwall
517 (Supplemental Fig. 5), and invoked this mechanism to explain unroofing of broad
518 expanses of mantle seen in the magma-poor rifted margins between Iberia and

519 Newfoundland. Capture of a portion of a previously rotated footwall section by a
520 second, successor fault in this way can increase the net rotation experienced by the
521 initial footwall, providing a mechanism capable of easily accommodating the
522 magnitude of early rotation seen in the Mersin ophiolite.
523
524 *5.2 Mode of formation and rotation of the metamorphic sole*
525
526 The later, post-magmatic net rotation affecting the metamorphic sole of the Mersin
527 ophiolite may have occurred: (i) in an intraoceanic, pre-obduction setting; (ii) during
528 emplacement onto the Tauride margin; or (iii) have a composite origin. However, the
529 consistency of rotation axes throughout the ophiolite is most simply explained by a
530 common tectonic process related to spreading.
531
532 Dykes cutting the sole have geochemical signatures indicating derivation from partial
533 melting of a depleted mantle wedge (Dilek *et al.,* 1999). Hence the metamorphic sole
534 must have been above this melt source during dyke intrusion, requiring a mechanism
535 for exhuming sole rocks from peak metamorphic depths to near the top of the mantle
536 wedge. Models for the formation of metamorphic soles involving intraoceanic
537 thrusting of young, hot oceanic lithosphere (e.g. Çelik, 2008) require dykes to intrude
538 through the complete footwall of the under-thrust lithosphere in order to be emplaced
539 into the metamorphic sole along the footwall-hanging wall contact. However, an
540 alternative model involving formation of metamorphic soles along the upper interface
541 of a down-going plate following subduction initiation and subsequent exhumation and
542 welding of the sole rocks to the base of overriding plate has recently been proposed
543 by van Hinsbergen et al. (2015). This model provides a mechanism for rapid

544 exhumation a newly-formed metamorphic sole to a position at the top of the mantle
545 wedge, allowing post-metamorphic dyke intrusion through the sole very shortly after
546 its formation. This is required in the case of the Tauride ophiolites, where ages of
547 dykes and metamorphic sole rocks typically differ in age by < 3 Myr (Table 1; Parlak
548 and Delaloye, 1996, 1999; Dilek *et al.,* 1999). The van Hinsbergen et al. (2015)
549 model involves slab flattening in response to formation and extension of the
550 suprasubduction zone crust, bringing sole rocks upwards to the base of the
551 overriding lithosphere, followed by slab steepening in response to negative buoyancy
552 resulting from eclogitization of the slab, leading to decoupling from the sole and influx
553 of asthenosphere below the sole from which the intruding dykes derive.
554
555 This model provides a critical link between early rotation of the Mersin cumulates and
556 mantle sequence dykes via fore-arc (hyper)extension involving oceanic detachment
557 faulting and later rotation of dykes cutting the Mersin metamorphic sole. Welding of
558 the metamorphic sole to the base of the mantle section via slab flattening would allow
559 these rocks to be captured in the base of detachment fault footwall sections. This
560 would allow rotation of the sole rocks around similar ridge-parallel, shallowly-plunging
561 axes to those documented in the overlying ophiolite. As well as accounting for the
562 similarity of rotation axes through the sampled units, this mechanism can also
563 account for the rapid sequence of rotations required by our data, with all phases of
564 rotation occurring over a restricted time interval of <~3 Myr during which crustal
565 accretion, formation of the sole and dyke emplacement occurred.
566
567 *5.3 A conceptual model for rotation of an ophiolite and its metamorphic sole in a fore-*
568 *arc environment*

Linking the upper plate process of fore-arc hyperextension (Maffione *et al.,* 2015) with the lower plate process of metamorphic sole formation and exhumation (van Hinsbergen *et al.,* 2015) leads to a combined conceptual model (Fig. 7) that can elegantly explain rapid, near-synchronous rotation of crust, mantle and sole around consistent ridge-parallel axes. This involves the following sequence of events:

a) initiation of an intraoceanic subduction zone, resulting concurrently in the early stages of formation of the future metamorphic sole (along the upper interface of the down-going plate) and suprasubduction zone spreading in the fore-arc region above the mantle wedge. This initial phase of magmatic spreading generates cumulate gabbros in the new suprasubduction zone lower crust and emplacement of dykes in the lithospheric mantle below (Fig. 7a);

b) amagmatic detachment-mode suprasubduction spreading, resulting in rotation of cumulate gabbros and mantle-hosted dykes in the footwall of an oceanic detachment fault (D1; Fig. 7b);

c) lack of melt supply leads to migration of the D1 detachment towards the locus of rifting (Tucholke et al., 2008; Reston and McDermott, 2011; MacLeod *et al.,* 2009), followed by initiation of a successor detachment (D2; Fig. 7c) that captures part of the rotated D1 footwall. Displacement on D2 then increases the rotation experienced by the cumulates and mantle-hosted dykes. At the same time, the down-going plate experiences slab flattening in response to suprasubduction zone spreading, mantle wedge volume decrease and upper

plate extension, leading to shallowing of the future metamorphic sole and development of its inverted pressure-temperature gradient (van Hinsbergen *et al.*, 2015);

d) at the plate contact, the metamorphic rocks at the top of the lower plate are welded to the base of the upper plate to form the metamorphic sole. Eclogitization of the lower plate then results in negative buoyancy and the initiation of slab pull, resulting in decoupling from the sole and steepening of the slab. Influx of asthenospheric mantle into the wedge generates melt and leads to intrusion of dykes into the emplaced metamorphic sole (Fig. 7d); and

e) further displacement on the D2 detachment results in additional rotation of the cumulate gabbros and mantle-hosted dykes and in disruption of the metamorphic sole, part of which rotates in the D2 footwall (Fig. 7e).

6. Conclusions

Net tectonic rotation analysis of paleomagnetic data from the suprasubduction Mersin ophiolite reveals large rotations around shallowly-plunging rotation axes that are consistently oriented NE-SW, parallel to the inferred orientation of the Neotethyan spreading axis. The data are best explained by combining recent concepts of detachment-mode spreading (leading to fore-arc hyperextension; Maffione *et al.,* 2015) and the formation and exhumation of metamorphic soles (van Hinsbergen *et al.,* 2015). Rotation of both the ophiolite and its metamorphic sole are inferred to be linked to rolling hinge rotation of detachment footwalls, as seen in oceanic core

complexes in modern (ultra-)slow spread lithosphere. This mode of spreading can also explain the absence of sheeted dyke complexes in several Upper Cretaceous Tauride ophiolites, as detachment-mode spreading characteristically results in tectonic juxtaposition of lower crustal and upper mantle rocks in detachment footwalls with upper crustal lavas in their hanging walls. Our results suggest that metamorphic sole rocks exhumed from peak metamorphic depths to the base of the suprasubduction zone lithosphere are then rotated as part of the upper plate. In addition, similar ages of crust and of dykes hosted in both the mantle and metamorphic sole require suprasubduction zone spreading, metamorphic sole exhumation, dyke emplacement and tectonic rotation to be essentially synchronous processes in a dynamic, intraoceanic fore-arc environment.

Acknowledgements

We thank the Ministry of Higher Education and Scientific Research (Iraq) for providing support for Ahmed Omer via a PhD scholarship held at Plymouth University. DJJvH acknowledges ERC Starting Grant 306810 (SINK) and NWO Vidi grant 864.11.004. Grateful thanks also to Osman Parlak for introducing us to the field geology of the Mersin ophiolite and for arranging field assistance by Çukurova University students during sampling. Net tectonic rotation analyses used the paleomagnetism.org application (Koymans *et al.,* 2016). Stereographic projections and Bingham statistics were produced using Richard Allmendinger's Stereonet program v. 9.9.4 (Cardozo *et al.,* 2013).

644 **References**

645 Allerton, S. and Vine, F. J., 1987. Spreading structure of the Troodos ophiolite,
646 Cyprus: some palaeomagnetic constraints. *Geology*, **15**, 593-597.

647 Cannat, M., Sauter, D., Mendel, V., Ruellan, E., Okino, K., Escartín, J., Combier, V.
648 and Baala, M., 2006. Modes of seafloor generation at a melt-poor ultraslow-
649 spreading axis. *Geology*, **34**, 605-608, doi: 10.1130/G22486.1.

650 Cardozo, N. and Allmendinger, R. W., 2013, Spherical projections with
651 OSXStereonet. *Computers & Geosciences*, **51**, 193 - 205, doi:
652 10.1016/j.cageo.2012.07.021.

653 Çelik, Ö., 2008. Detailed Geochemistry and K-Ar Geochronology of the Metamorphic
654 Sole Rocks and Their Mafic Dykes from the Mersin Ophiolite, Southern Turkey.
655 *Turkish Journal of Earth Sciences*, **17**, 685-708.

656 Clube, T., Creer, K. and Robertson, A., 1985. Palaeorotation of the Troodos
657 microplate, Cyprus, *Nature*, **317**, 522-525.

658 Deenen, M. H. L., Langereis, C. G., van Hinsbergen, D. J. J. and Biggin, A. J., 2011.
659 Geomagnetic secular variation and the statistics of palaeomagnetic directions.
660 *Geophysical Journal International*, **186**, 509-520.

661 Dilek, Y., Thy, P., Hacker, B. and Grundvig, S., 1999. Structure and petrology of
662 Tauride ophiolites and mafic dike intrusions (Turkey): Implications for the Neotethyan
663 ocean. *Geological Society of America Bulletin*, **111**, 1192.

664 Escartín, J. and Canales, J. P., 2011. Detachments in oceanic lithosphere:
665 Deformation, magmatism, fluid flow, and ecosystems. *Eos Trans. AGU*, **92**, 31.

666 Garcés, M. and Gee, J. S., 2007. Paleomagnetic evidence of large footwall rotations
667 associated with low-angle faults at the Mid-Atlantic Ridge. *Geology,* **35**, 279–282.

668 Gee, J. S. and Kent, D. V., 2007. Source of oceanic magnetic anomalies and the
669 geomagnetic polarity time scale. *Treatise on Geophysics*, **5**, 455-507.

670 Granot, R., Abelson, M., Ron, H., Lusk, M. W. and Agnon, A., 2011. Direct evidence
671 for dynamic magma supply fossilized in the lower oceanic crust of the Troodos
672 ophiolite. *Geophysical Research Letters*, **38**, L16311, doi: 10.1029/2011GL048220.

673 Gurnis, M., Hall, C. and Lavier, L., 2004. Evolving force balance during incipient
674 subduction. *Geochemistry, Geophysics, Geosystems*, **5**, Q07001, doi:
675 10.1029/2003GC000681.

676 Hacker, B. R. and Gnos, E., 1997. The conundrum of Samail: explaining the
677 metamorphic history. *Tectonophysics*, **279**, 215-226.

678 Hurst, S. D., Verosub, K. L. and Moores, E. M., 1992. Paleomagnetic constraints on
679 the formation of the Solea graben, Troodos ophiolite, Cyprus. *Tectonophysics*, **208**,
680 431–445, doi: 10.1016/0040-1951(92)90439-D.

681 Inwood, J., Morris, A., Anderson, M. W. and Robertson, A. H. F., 2009. Neotethyan
682 intraoceanic microplate rotation and variations in spreading axis orientation:
683 Palaeomagnetic evidence from the Hatay ophiolite (southern Turkey). *Earth and*
684 *Planetary Science Letters*, **280**, 105-117.

685 Johnson, C.L., Constable, C. G., Tauxe, L., Barendregt, R., Brown, L. L., Coe, R. S.,
686 Layer, P., Mejia, V., Opdyke, N. D., Singer, B. S., Staudigel, H. and Stone, D. B.,
687 2008. Recent investigations of the 0–5 Ma geomagnetic field recorded by lava flows.
688 *Geochemistry, Geophysics, Geosystems*, **9**, Q04032, doi: 10.1029/2007GC001696.

689 Koymans, M.R., Langereis, C.G., Pastor-Galan, D. and van Hinsbergen, D.J.J.,
690 2016. Paleomagnetism.org: An online multi-platform open source environment for
691 paleomagnetic data analysis. *Computers and Geosciences*, **93**, 127–137.

692 MacDonald, W. D., 1980. Net tectonic rotation, apparent rotation, and the structural
693 tilt correction in palaeomagnetic studies. *Journal of Geophysical Research*, **85**, 3659-
694 3669.

695 MacLeod, C., Allerton, S., Gass, I. and Xenophontos, C., 1990. Structure of a fossil
696 ridge–transform intersection in the Troodos ophiolite. *Nature*, **348**, 717-720.

697 MacLeod, C. J., Searle, R. C., Murton, B. J., Casey, J. F., Mallows, C. Unsworth,
698 S.C., Achenbach, K. L. and Harris, M., 2009. Life cycle of oceanic core complexes.
699 *Earth and Planetary Science Letters*, **287**, 333-344, doi: 10.1016/j.epsl.2009.08.016..

700 MacLeod, C. J., Carlut, J., Escartín, J., Horen, H. and Morris, A., 2011. Quantitative
701 constraint on footwall rotations at the 15°45'N oceanic core complex, Mid-Atlantic
702 Ridge: implications for detachment fault processes. *Geochemistry, Geophysics,*
703 *Geosystems*, **12**, Q0AG03, doi: 10.1029/2011GC003503.

704 MacLeod, C.J., Dick, H.J.B., Blum, P. and the Expedition 360 Scientists,
705 2017. *Southwest Indian Ridge Lower Crust and Moho.* Proceedings of the
706 International Ocean Discovery Program, 360: College Station, TX (International
707 Ocean Discovery Program), doi: 10.14379/iodp.proc.360.2017.

708 Maffione, M., Morris, A. and Anderson, M. W., 2013. Recognizing detachment-mode
709 spreading in the deep geological past. *Scientific Reports*, 3:2336, doi:
710 10.1038/srep02336.

Maffione, M., van Hinsbergen, D. J. J., Koornneef, L. M. T., Guilmette, C., Hodges, K., Borneman, N., Huang, W., Ding, L., and Kapp, P., 2015. Forearc hyperextension dismembered the south Tibetan ophiolites. *Geology*, **43**, 475–478, doi: 10.1130/G36472.1.

Maffione, M., van Hinsbergen, D., de Gelder, G., van der Goes, F. & Morris, A., 2017. Kinematics of Late Cretaceous subduction initiation in the Neo-Tethys Ocean reconstructed from ophiolites of Turkey, Cyprus, and Syria. *Journal of Geophysical Research: Solid Earth*, doi: 10.1002/2016JB013821

Morris, A. and Anderson, M. W., 2002, Palaeomagnetic results from the Baër-Bassit ophiolite of northern Syria and their implication for fold tests in sheeted dyke terrains. *Physics and Chemistry of the Earth*, **27**, 1215-1222.

Morris, A. and Maffione, M., 2016. Is the Troodos ophiolite (Cyprus) a complete, transform fault-bounded Neotethyan ridge segment?, *Geology*, **44**, 199–202, doi:10.1130/G37529.1.

Morris, A., Creer, K. M. and Robertson, A. H. F., 1990. Palaeomagnetic evidence for clockwise rotations related to dextral shear along the Southern Troodos Transform Fault, Cyprus. *Earth and Planetary Science Letters*, **99**, 250-262.

Morris, A., Anderson, M. W. and Robertson, A. H. F., 1998. Multiple tectonic rotations and transform tectonism in an intra-oceanic suture zone, SW Cyprus. *Tectonophysics*, **299**, 229-253.

Morris, A., Anderson, M. W., Robertson, A. H. F. and Al-Riyami, K., 2002. Extreme tectonic rotations within an eastern Mediterranean ophiolite (Baër -Bassit, Syria). *Earth and Planetary Science Letters*, **202**, 247–261, doi:10.1016/S0012-821X(02)00782-3.

735 Morris, A., Gee, J. S., Pressling, N., John, B. E., MacLeod, C. J., Grimes, C. B. and
736 Searle, R. C., 2009. Footwall rotation in an oceanic core complex quantified using
737 reorientated Integrated Ocean Drilling Program core samples. *Earth and Planetary*
738 *Science Letters,* **287**, 217-228, doi: 10.1016/j.epsl.2009.08.007.

739 Parlak, O. and Delaloye, M., 1996. Geochemistry and timing of post metamorphic
740 dyke emplacement in the Mersin Ophiolite (southern Turkey): New age constraints
741 from 40Ar/39Ar geochronology. *Terra Nova*, **8**, 585-592.

742 Parlak, O. and Delaloye, M., 1999. Precise 40Ar/39Ar ages from the metamorphic
743 sole of the Mersin ophiolite (southern Turkey). *Tectonophysics*, **301**, 145-158.

744 Parlak, O., Delaloye, M., and Bingöl, E., 1996a. Mineral chemistry of ultramafic and
745 mafic cumulates as an indicator of the arc-related origin of the Mersin ophiolite
746 (southern Turkey). *Geol. Rundsch.*, **85**, 647-661.

747 Parlak, O., Bozkurt, E. and Delaloye, M., 1996b. The obduction direction of the
748 Mersin Ophiolite: structural evidence from subophiolitic metamorphics in the Central
749 Tauride Belt, Southern Turkey. *International Geology Review*, **38**, 778-786.

750 Parlak, O., Karaoğlan, F., Rızaoğlu, T., Klötzli, U., Koller, F. and Billor, Z., 2013. U-
751 Pb and ^{40}Ar–^{39}Ar geochronology of the ophiolites and granitoids from the Tauride
752 belt: Implications for the evolution of the Inner Tauride suture. *Journal of*
753 *Geodynamics*, **65**, 22– 37.

754 Pearce, J. A. and Robinson, P. T., 2010. The Troodos ophiolitic complex probably
755 formed in a subduction initiation, slab edge setting. *Gondwana Research*, **18**, 60-81,
756 doi: 10.1016/j.ge.2009.12.003.

757 Petrovský, E. and Kapička, A., 2006. On determination of the Curie point from
758 thermomagnetic curves. *Journal of Geophysical Research*, **111**, 1-10.

759 Reston. T. J. and McDermott, K. G., 2011. Successive detachment faults and mantle
760 unroofing at magma-poor rifted margins. *Geology*, **39**, 1071-1074, doi:
761 10.1130/G32428.1.

762 Robertson, A. H. F., 2002. Overview of the genesis and emplacement of Mesozoic
763 ophiolites in the Eastern Mediterranean Tethyan region. *Lithos*, **65**,1-67.

764 Salisbury, M. H. and Keen, C. E., 1993. Listric faults imaged in oceanic crust.
765 *Geology***, 21**, 117-120, doi: 10.1130/0091-7613(1993)021<0117:LFIIOC>2.3.CO;2.

766 Smith, D. K., Escartín, J., Schouten, H., Cann, J. R., 2008. Fault rotation and core
767 complex formation: significant processes in seafloor formation at slow-spreading mid-
768 ocean ridges (Mid-Atlantic Ridge, 13°–15°N). *Geochem. Geophys. Geosyst*., **9**,
769 Q03003. doi:10.1029/2007GC001699.

770 Staudigel, H., Gee, J. and Tauxe, L., 1992. Shallow intrusive directions of sheeted
771 dikes in the Troodos ophiolite: Anisotropy of magnetic susceptibility and structural
772 data. *Geology*, **20**, 841-844.

773 Stern, R. J. and Bloomer, S. H., 1992. Subduction zone infancy: Examples from he
774 Eocene Izu-Bonin-Mariana and Jurassic California arcs. *Geol. Soc. Am. Bull.*, **104**,
775 1621-1636.

776 Tekin, U. K., Bedi, Y., Okuyucu, C., Göncüoglu, M. C. and Sayit, K., 2016.
777 Radiolarian biochronology of upper Anisian to upper Ladinian (Middle Triassic)
778 blocks and tectonic slices of volcano-sedimentary successions in the Mersin

779 Mélange, southern Turkey: New insights for the evolution of Neotethys. *Journal of*
780 *African Earth Sciences*, **124**, 409-426, doi: 10.1016/j.jafrearsci.2016.09.039.

781 Torsvik, T. H., Van der Voo, R., Preeden, U., Mac Niocaill, C., Steinberger, B.,
782 Doubrovine, P. V., van Hinsbergen, D. J., Domeier, M., Gaina, C. & Tohver, E., 2012.
783 Phanerozoic polar wander, palaeogeography and dynamics. *Earth-Science Reviews*,
784 **114**, 325–368, doi: 10.1016/j.earscirev.2012.06.002.

785 Tucholke, B. E., Behn, M. D., Buck, W. R. and Lin, J., 2008. Role of melt supply in
786 oceanic detachment faulting and formation of megamullions. *Geology*, 36, 455–458,
787 doi:10.1130/G24639A.1.

788 van Hinsbergen, D. J. J., Peters, K., Maffione, M., Spakman, W., Guilmette, C.,
789 Thieulot, C., Plümper, O., Gürer, D., Brouwer, F. M., Aldanmaz, E. and Kaymakcı, N.,
790 2015. Dynamics of intraoceanic subduction initiation: 2. Suprasubduction zone
791 ophiolite formation and metamorphic sole exhumation in context of absolute plate
792 motions. *Geochem. Geophys. Geosyst.*, **16**, doi:10.1002/ 2015GC005745.

793 van Hinsbergen, D. J. J., Maffione, M., Plunder, A., Kaymakcı, N., Ganerød, M.,
794 Hendriks, B. W. H., Corfu, F., Gürer, D., de Gelder, G. I. N. O., Peters, K., McPhee,
795 P. J., Brouwer, F. M., Advokaat, E. L. and Vissers, R. L. M., 2016. Tectonic evolution
796 and paleogeography of the Kırşehir Block and the Central Anatolian Ophiolites,
797 Turkey. *Tectonics*, **35**, 983-1014, doi: 10.1002/2015TC004018.

798 Varga, R. J. and Moores, E. M., 1985. Spreading structure of the Troodos ophiolite,
799 Cyprus. *Geology*, **13**, 846-850, doi: 10.1130/0091-
800 7613(1985)13<846:SSOTTO>2.0.CO;2.

801

802 **Figure captions**

Fig. 1. Summary of the geology of the Mersin ophiolite of southern Turkey. (a) Simplified geological map (after Tekin *et al.,* 2016); (b) tectonostratigraphic column (after Parlak *et al.,* 1996b). In this study we have sampled dykes cutting the metamorphic sole of the ophiolite, dykes cutting the mantle sequence, and ultramafic and gabbroic cumulates of the lower crust for paleomagnetic analysis. (a color version of this figure is available with the web version of the article).

Fig. 2. (a) Modal compositional layering in cumulate gabbros exposed along the Sorgun valley in the Mersin ophiolite (site MC09; compass-clinometer for scale). (b) Close-up of modal layering (coin for scale). In this example, compositional grading from olivine-rich bases to plagioclase-rich tops (X) combined with scour structures (dashed lines) provide way-up indicators that indicate overturning of the section. Darker area (Y) is a remnant of a thin (< 3 cm thick) basaltic dyke cutting the gabbros (sampled as site MC10).

Fig. 3. (a) High-temperature variations of low-field magnetic susceptibility (*k*) showing maximum Curie temperatures of ~580°C. Inset diagrams show the variation of 1/*k,* allowing accurate determination of Curie temperatures using the Petrovsky and Kapička (2006) method. (b) Isothermal remanent magnetization (IRM) acquisition curves showing presence of low coercivity magnetite.

Fig. 4. Typical examples of orthogonal demagnetization diagrams, showing well-defined, characteristic remanence directions isolated by both alternating field (AF)

827 and thermal (Th) treatment in all lithologies. Solid circles = horizontal plane; open
828 symbols = vertical N-S or E-W plane.
829
830 Fig.5. Net tectonic rotation results from the Mersin ophiolite, combining site-level
831 preferred solutions from each lithostratigraphic unit. (a) histograms of rotation angles;
832 (b) contoured equal area stereographic projections of rotation axes; and (c) rose
833 diagrams of restored initial dyke strikes. Note that rotation axes are consistently NE-
834 SE-directed and parallel to initial dyke strikes. Inset diagrams show the results for
835 early rotation of the dykes cutting the mantle section and for lower crustal cumulates
836 found by back-stripping the mean net tectonic rotation determined from dykes in the
837 metamorphic sole (representing the latest component of rotation in the Mersin
838 ophiolite).
839 (a color version of this figure is available with the web version of the article).
840
841 Fig. 6. Equal area stereographic projections comparing (a) the style of the early
842 rotation of the cumulate and mantle-hosted dykes of the Mersin ophiolite with footwall
843 rotations documented in (b) the Atlantis Massif (Morris *et al.,* 2009) and (c) 15°45'N
844 (MacLeod *et al.,* 2011) OCCs on the Mid Atlantic Ridge (MAR) and in (d) a fossil
845 OCC preserved in the Mirdita ophiolite of Albania (Maffione *et al.,* 2013). The results
846 for the Mersin ophiolite shown here represents an average amalgamating all net
847 tectonic rotations solutions after back-stripping the effects of the later rotation of the
848 metamorphic sole. Note that in all cases, rotation axes are shallowly-plunging and
849 parallel to the observed or inferred orientation of the associated spreading axis.
850
851

852 Fig. 7. Conceptual model for rapid and extreme tectonic rotation of a
853 suprasubduction zone ophiolite and its metamorphic sole in a fore-arc environment
854 (see text for details). Note that detachment-mode spreading in the upper plate may
855 involve development of multiple oceanic detachment faults, but the model shows only
856 the minimum number of structures required to explain the Mersin paleomagnetic
857 data.
858 (a color version of this figure is available with the web version of the article).
859
860 Table 1. Summary of geochronological constraints from the Mersin ophiolite.
861
862 Table 2. Paleomagnetic results from the Mersin ophiolite. Orientation of
863 paleosurfaces (dyke margins; cumulate layering) are expressed as dip direction/dip.
864 O/T = overturned. D, I, declination and inclination of *in situ* site mean remanence.
865 ΔD, ΔI, declination and inclination error, respectively. k, α_{95}, precision parameter and
866 95% cone of confidence around the site mean characteristic remanent
867 magnetizations (ChRMs). K, A_{95}, precision parameter and 95% cone of confidence
868 around the site mean virtual geomagnetic pole (VGP). A_{95min}, A_{95max}, minimum and
869 maximum value of A_{95} expected from paleosecular variation of the geomagnetic field,
870 according to Deenen et al. (2011). N, number of total samples used for the statistics.
871
872 Table 3. Net tectonic rotation parameters for dykes and cumulate rocks of the Mersin
873 ophiolite
874
875 Supplemental Fig. 1. Equal area stereographic projections summarizing
876 paleomagnetic results obtained from sites in the Mersin ophiolite. Blue circles =

877 specimen characteristic remanent magnetizations (ChRMs, top projections, with
878 closed/open symbols indicating directions on the lower/upper hemispheres
879 respectively) or corresponding virtual geomagnetic poles (VGPs, with mean rotated
880 to vertical, bottom projections); green diamond = present day field direction
881 (inclination = 56°); orange square = Late Cretaceous reference direction (inclination =
882 40.2°); black circles = site mean magnetization directions; red circles = α_{95}/A_{95} cones
883 of confidence on site mean magnetizations/VGP distributions, respectively; dashed
884 line = 45° cut-off on VGP distributions (following Johnson *et al.,* 2008). See Table 1
885 for details of site locations and lithologies.
886
887 Supplemental Fig. 2. Illustration of the net tectonic rotation algorithm employed in this
888 study, based on the Allerton and Vine (1987) method for (a) the paleovertical (dyke)
889 case and (b) the paleohorizontal (layered gabbro) case. SMV = site magnetization
890 vector (*in situ* remanence); RMV = reference magnetization vector; PDP = present
891 day pole to paleosurface; IP = initial pole to paleosurface; RP = axis of net tectonic
892 rotation; dotted line indicates circle of radius β (= angle between SMV and PDP)
893 centred on RMV; dashed lines indicate great circles that bisect the pairs of vectors;
894 subscripts 1 and 2 refer to alternative solutions in the dyke case, whereas the
895 paleohorizontal case gives only one solution. Multiple application of this method for
896 (c) the paleovertical and (d) paleohorizontal cases using all combinations of five
897 estimates of SMV and PDP and three estimates of RMV. This yields 75 estimates of
898 the rotation axis for each site, from which a mean estimate can be derived using
899 Bingham statistics. Inset histograms illustrate the associated distributions of net
900 tectonic rotation angles.
901

Supplemental Fig. 3. Net tectonic rotation results from individual dyke sites within the Mersin ophiolite. Results at each site are presented as a histogram of potential rotation angles, a contoured equal area stereographic projection of potential rotation axes and a rose diagram of restored initial dyke strikes.

Supplemental Fig. 4. Net tectonic rotation results from individual lower crustal cumulate sites within the Mersin ophiolite. Results at each site are presented as a histogram of potential rotation angles and a contoured equal area stereographic projection of potential rotation axes.

Supplemental Fig. 5. Accommodation of extreme rotation through displacement on successive oceanic detachment faults, based on the model of Reston and McDermott (2011). (a) Amagmatic extension is taken up on an oceanic detachment fault D1 rooted at the rift axis (grey arrow); (b) as the D1 footwall experiences rolling hinge rotation and is pulled out from beneath the hanging wall, the active fault root moves (white arrow) with the hanging wall over the rift axis; (c) the D1 detachment then becomes inactive and a new fault (D2) cuts up from the rift axis, capturing part of the rotated D1 footwall; (d) rolling hinge rotation of the D2 footwall increases the net rotation of the captured portion of the D1 footwall.

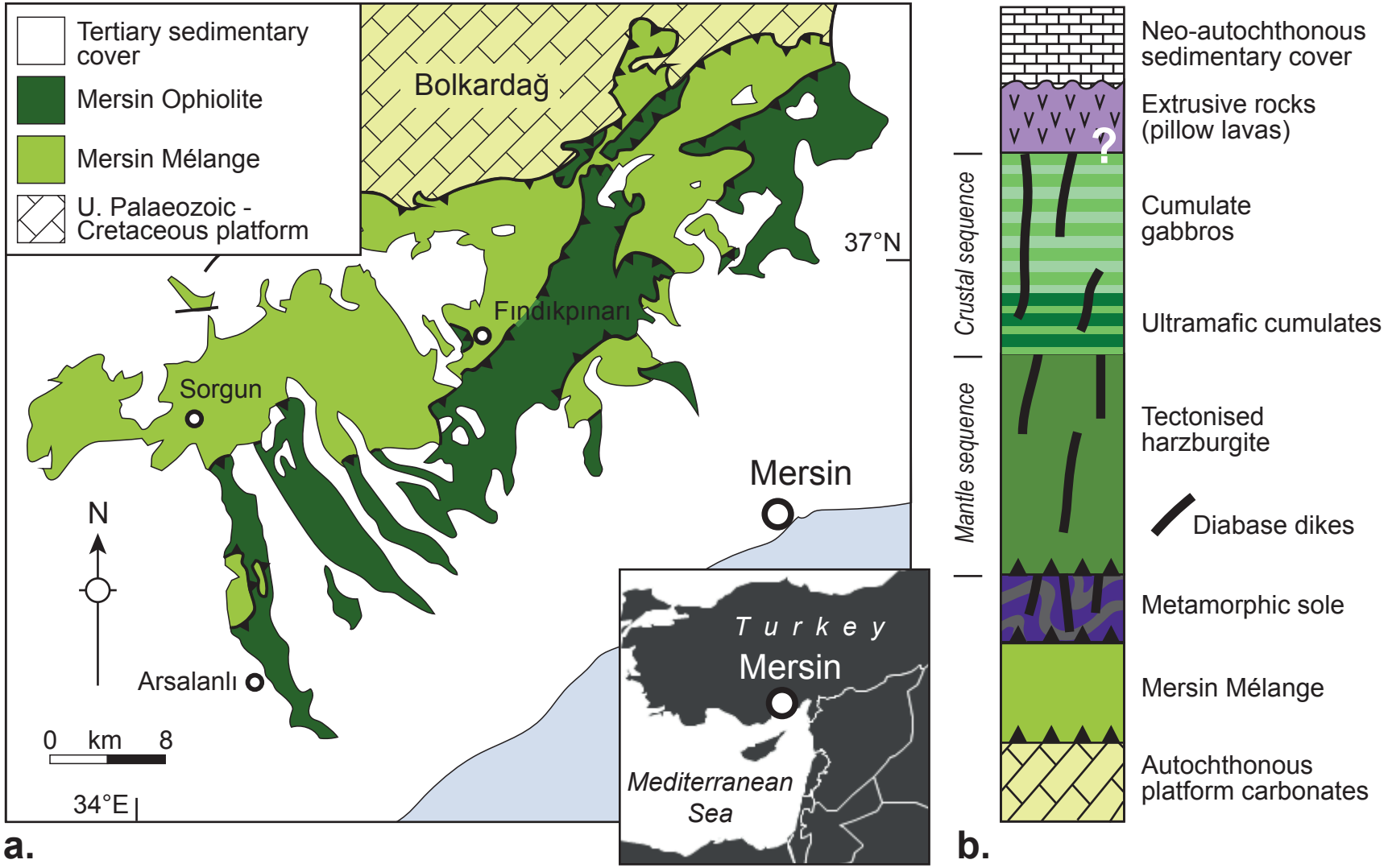
Tertiary sedimentary cover
Mersin Ophiolite
Mersin Mélange
U. Palaeozoic - Cretaceous platform
Bolkardağ
37°N
Fındıkpınarı
Sorgun
Mersin
N
Arsalanlı
0 km 8
34°E
Turkey
Mersin
Mediterranean Sea
a.
Neo-autochthonous sedimentary cover
Extrusive rocks (pillow lavas)
?
Crustal sequence
Cumulate gabbros
Ultramafic cumulates
Mantle sequence
Tectonised harzburgite
Diabase dikes
Metamorphic sole
Mersin Mélange
Autochthonous platform carbonates
b.

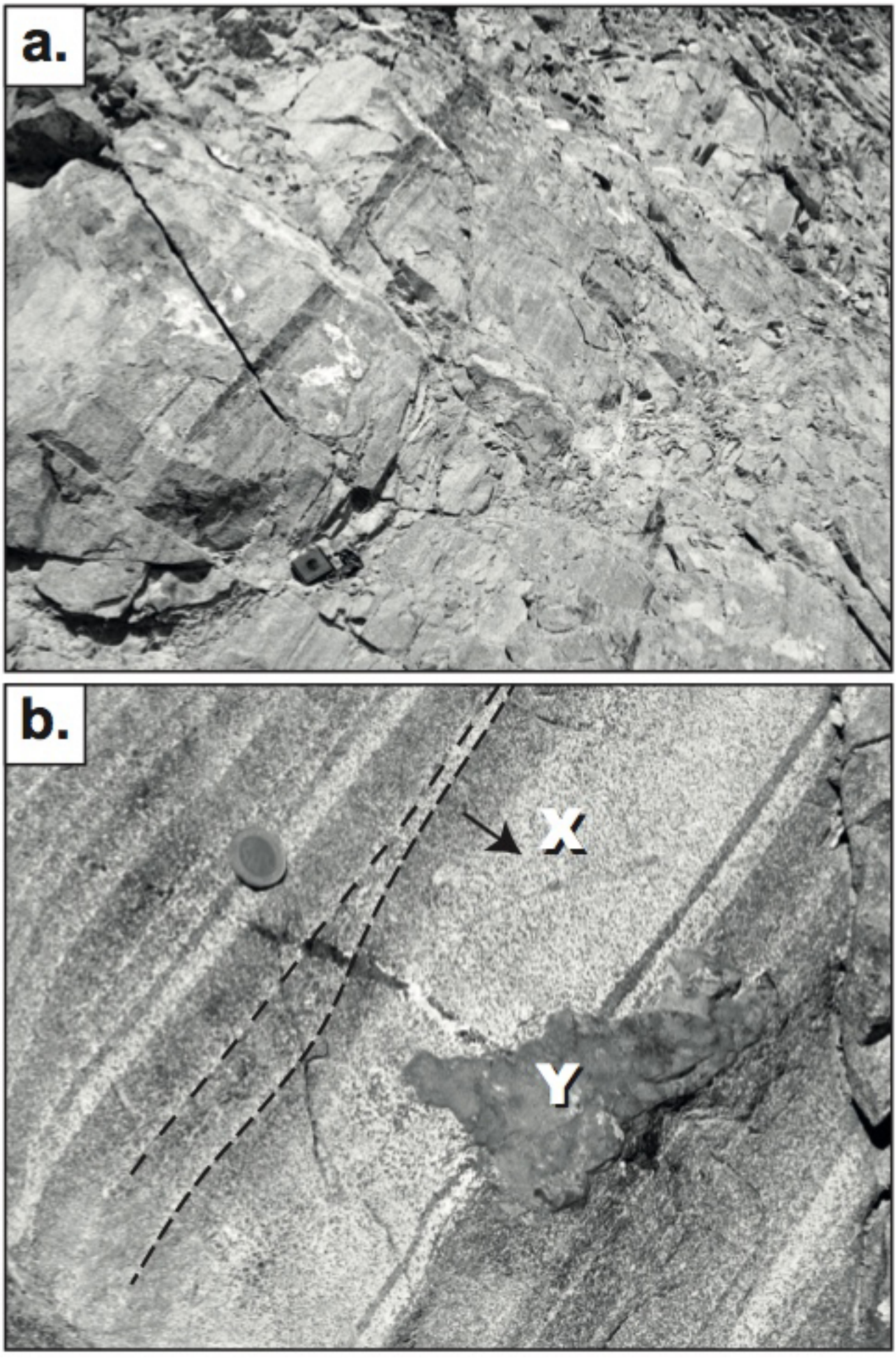
a.
b.
X
Y

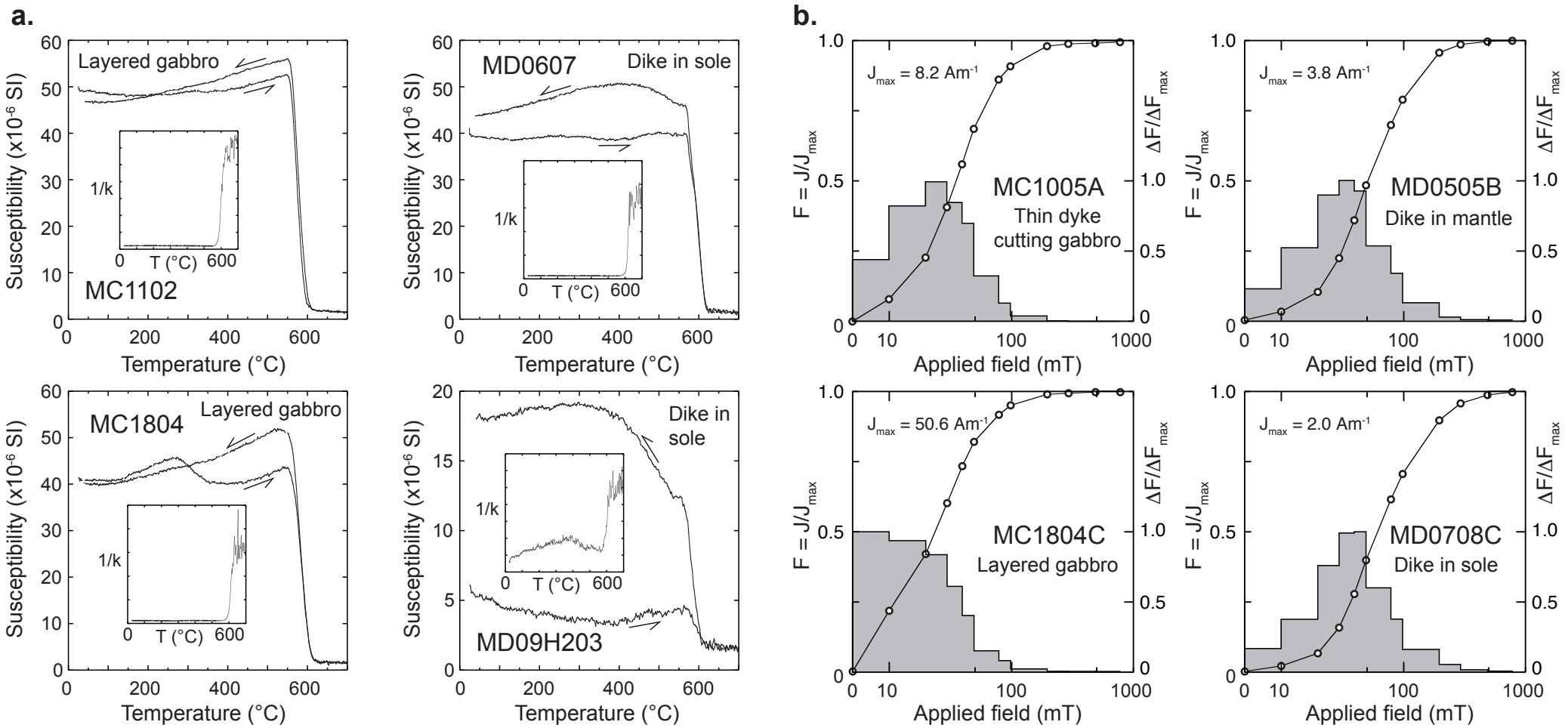
a.
Layered gabbro
MC1102
1/k
0 T (°C) 600
Susceptibility (x10-6 SI)
Temperature (°C)
MD0607
Dike in sole
MC1804
Layered gabbro
MD09H203
Dike in sole
b.
Jmax = 8.2 Am-1
MC1005A
Thin dyke cutting gabbro
Jmax = 3.8 Am-1
MD0505B
Dike in mantle
Jmax = 50.6 Am-1
MC1804C
Layered gabbro
Jmax = 2.0 Am-1
MD0708C
Dike in sole
F = J/Jmax
ΔF/ΔFmax
Applied field (mT)

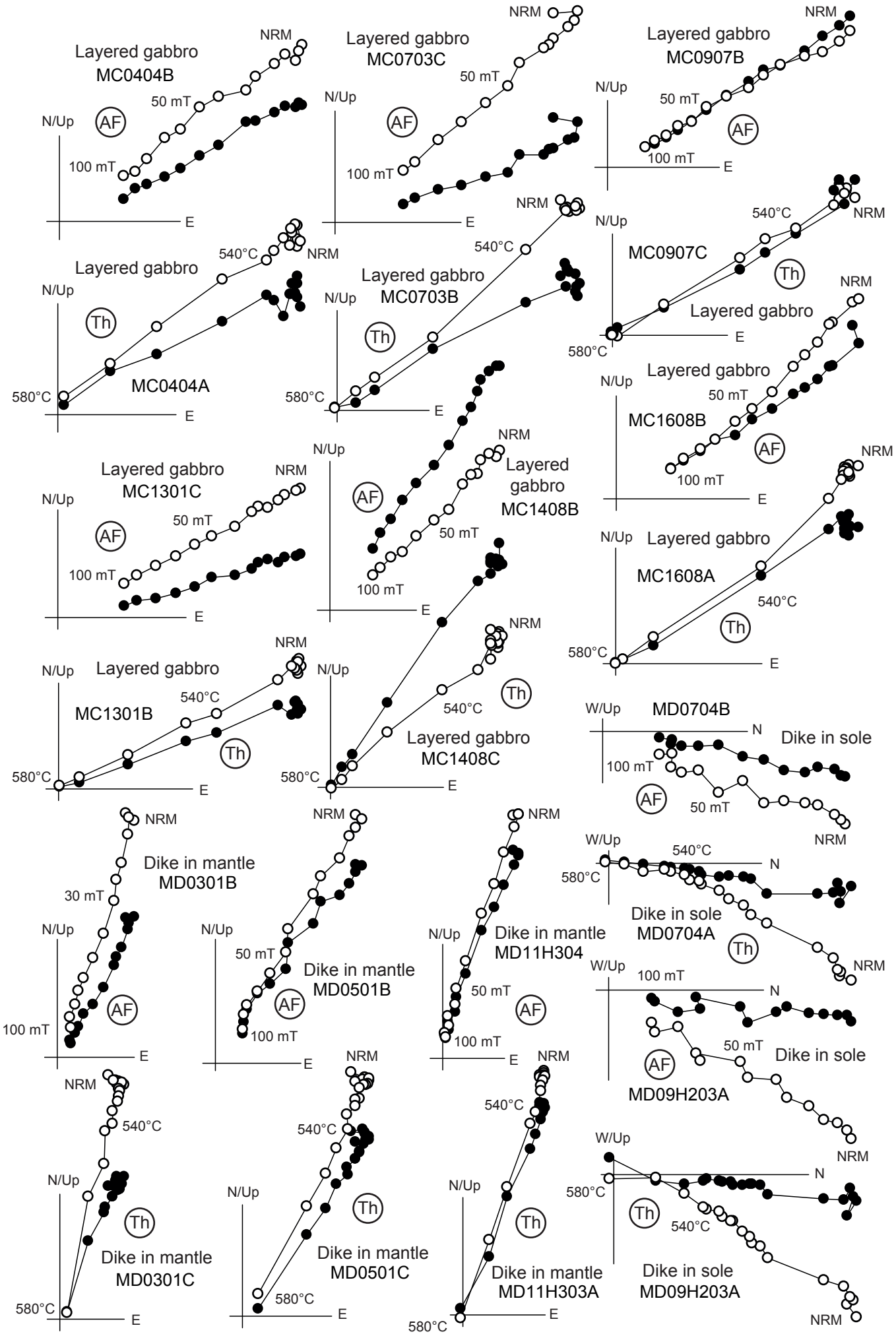
Layered gabbro
MC0404B
NRM
50 mT
N/Up
AF
100 mT
E
Layered gabbro
MC0703C
NRM
50 mT
N/Up
AF
100 mT
E
Layered gabbro
MC0907B
NRM
N/Up
50 mT
AF
100 mT
E
Layered gabbro
NRM
540°C
N/Up
Th
MC0404A
580°C
E
Layered gabbro
MC0703B
NRM
540°C
N/Up
Th
580°C
E
MC0907C
N/Up
540°C
NRM
Th
Layered gabbro
580°C
E
Layered gabbro
MC1608B
NRM
N/Up
50 mT
AF
100 mT
E
Layered gabbro
MC1301C
NRM
N/Up
AF
50 mT
100 mT
E
NRM
N/Up
AF
Layered
gabbro
MC1408B
50 mT
100 mT
E
Layered gabbro
MC1608A
N/Up
540°C
Th
580°C
E
Layered gabbro
MC1301B
NRM
N/Up
540°C
Th
580°C
E
NRM
N/Up
Th
540°C
Layered gabbro
MC1408C
580°C
E
W/Up
MD0704B
N
Dike in sole
100 mT
AF
50 mT
NRM
Dike in mantle
MD0301B
NRM
30 mT
N/Up
AF
100 mT
E
NRM
N/Up
50 mT
Dike in mantle
MD0501B
AF
100 mT
E
NRM
N/Up
Dike in mantle
MD11H304
50 mT
AF
100 mT
E
W/Up
540°C
N
580°C
Dike in sole
MD0704A
Th
NRM
W/Up
100 mT
N
50 mT
Dike in sole
AF
MD09H203A
NRM
540°C
N/Up
Th
Dike in mantle
MD0301C
580°C
E
NRM
540°C
N/Up
Th
Dike in mantle
MD0501C
580°C
E
NRM
540°C
N/Up
Th
Dike in mantle
MD11H303A
580°C
E
W/Up
NRM
N
580°C
Th
540°C
Dike in sole
MD09H203A
NRM

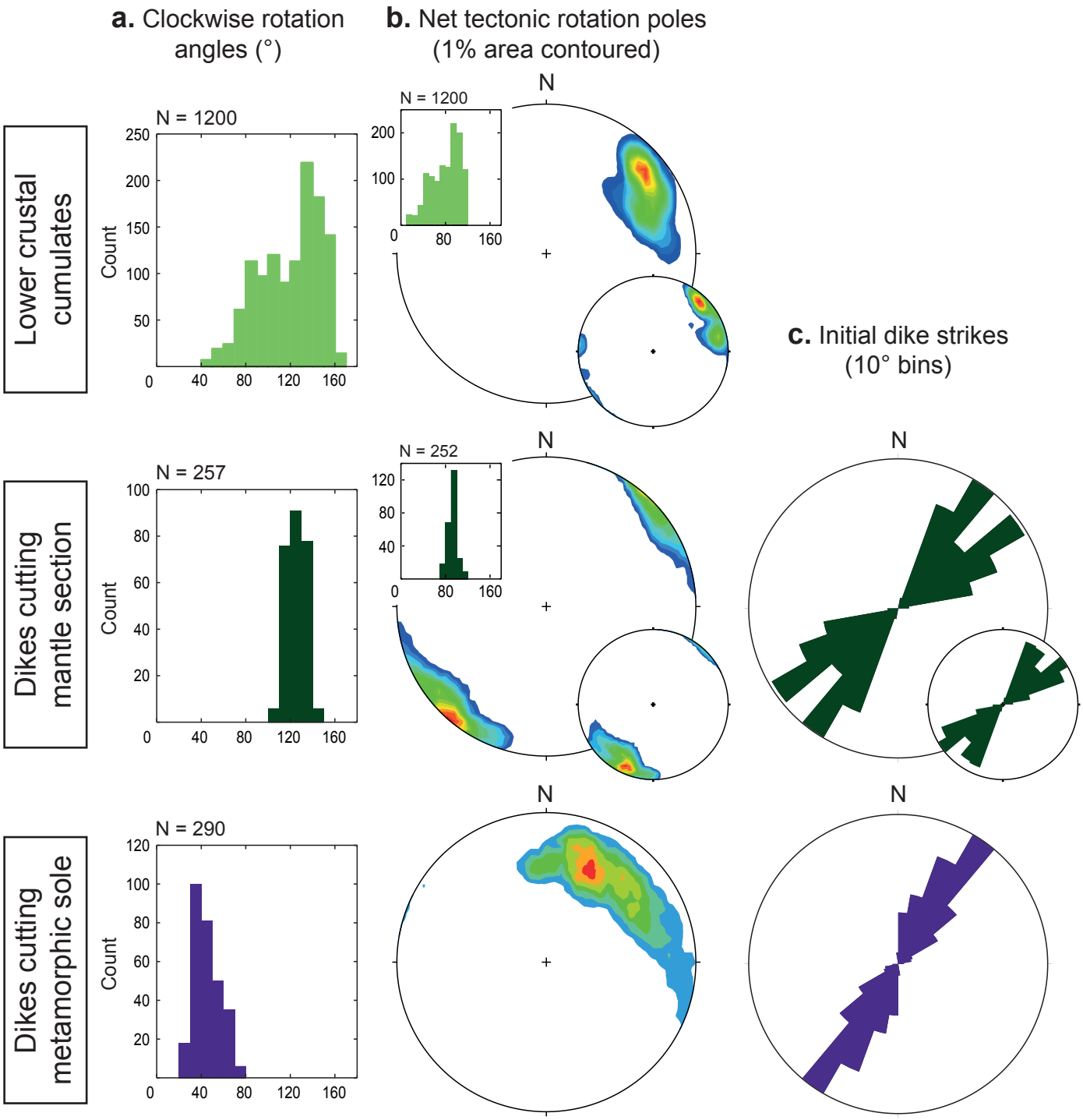
a. Clockwise rotation angles (°)
b. Net tectonic rotation poles (1% area contoured)
c. Initial dike strikes (10° bins)
Lower crustal cumulates
Dikes cutting mantle section
Dikes cutting metamorphic sole
N = 1200
N = 257
N = 290
N = 252
Count
N

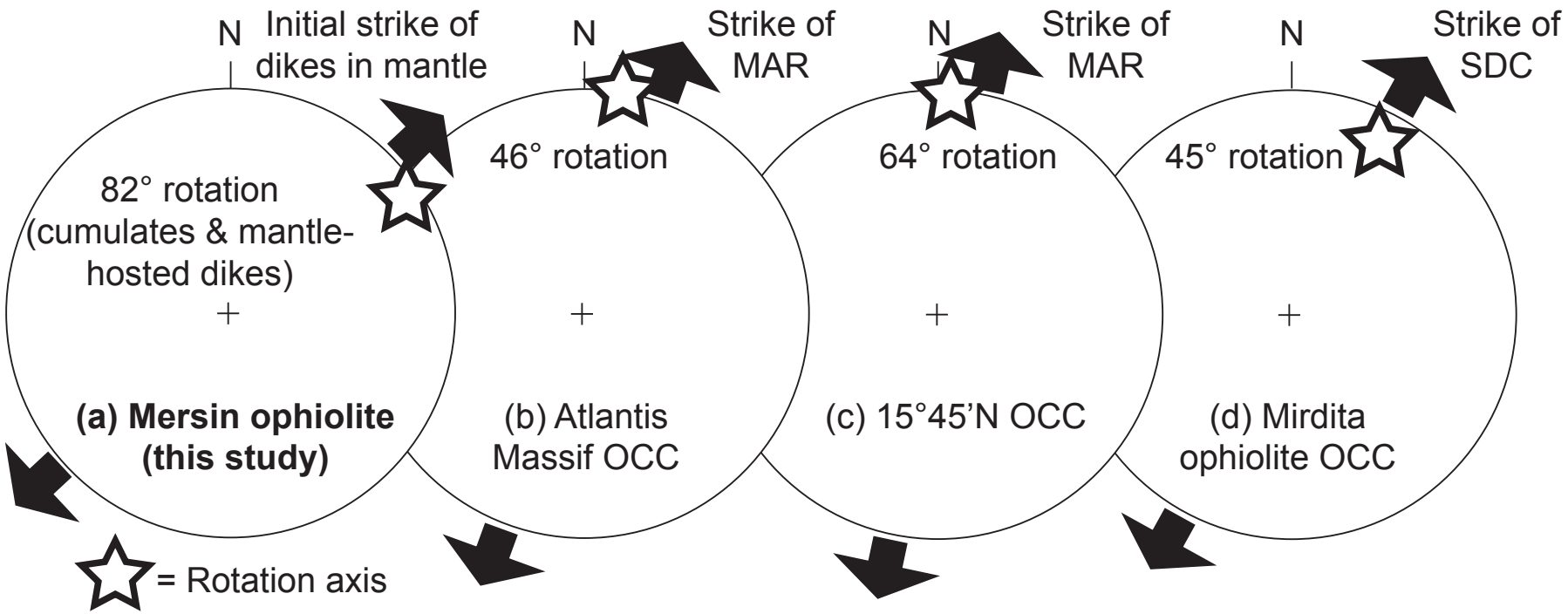
N
Initial strike of dikes in mantle
82° rotation (cumulates & mantle-hosted dikes)
(a) Mersin ophiolite (this study)
N
Strike of MAR
46° rotation
(b) Atlantis Massif OCC
N
Strike of MAR
64° rotation
(c) 15°45'N OCC
N
Strike of SDC
45° rotation
(d) Mirdita ophiolite OCC
= Rotation axis

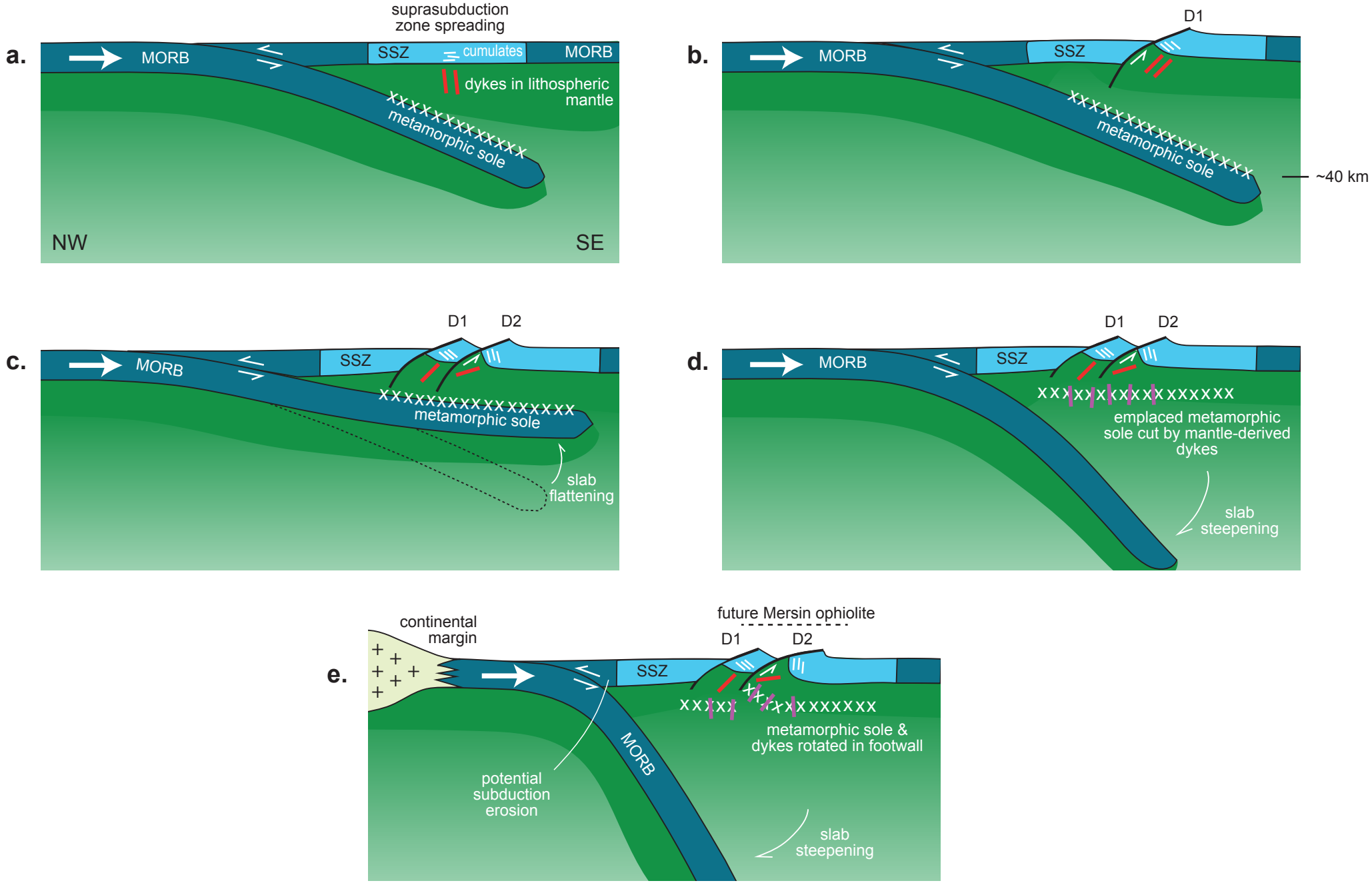
a.
suprasubduction zone spreading
MORB
SSZ
cumulates
MORB
dykes in lithospheric mantle
metamorphic sole
NW
SE
b.
D1
MORB
SSZ
metamorphic sole
~40 km
c.
D1
D2
MORB
SSZ
metamorphic sole
slab flattening
d.
D1
D2
MORB
SSZ
emplaced metamorphic sole cut by mantle-derived dykes
slab steepening
e.
continental margin
future Mersin ophiolite
D1
D2
SSZ
metamorphic sole & dykes rotated in footwall
MORB
potential subduction erosion
slab steepening

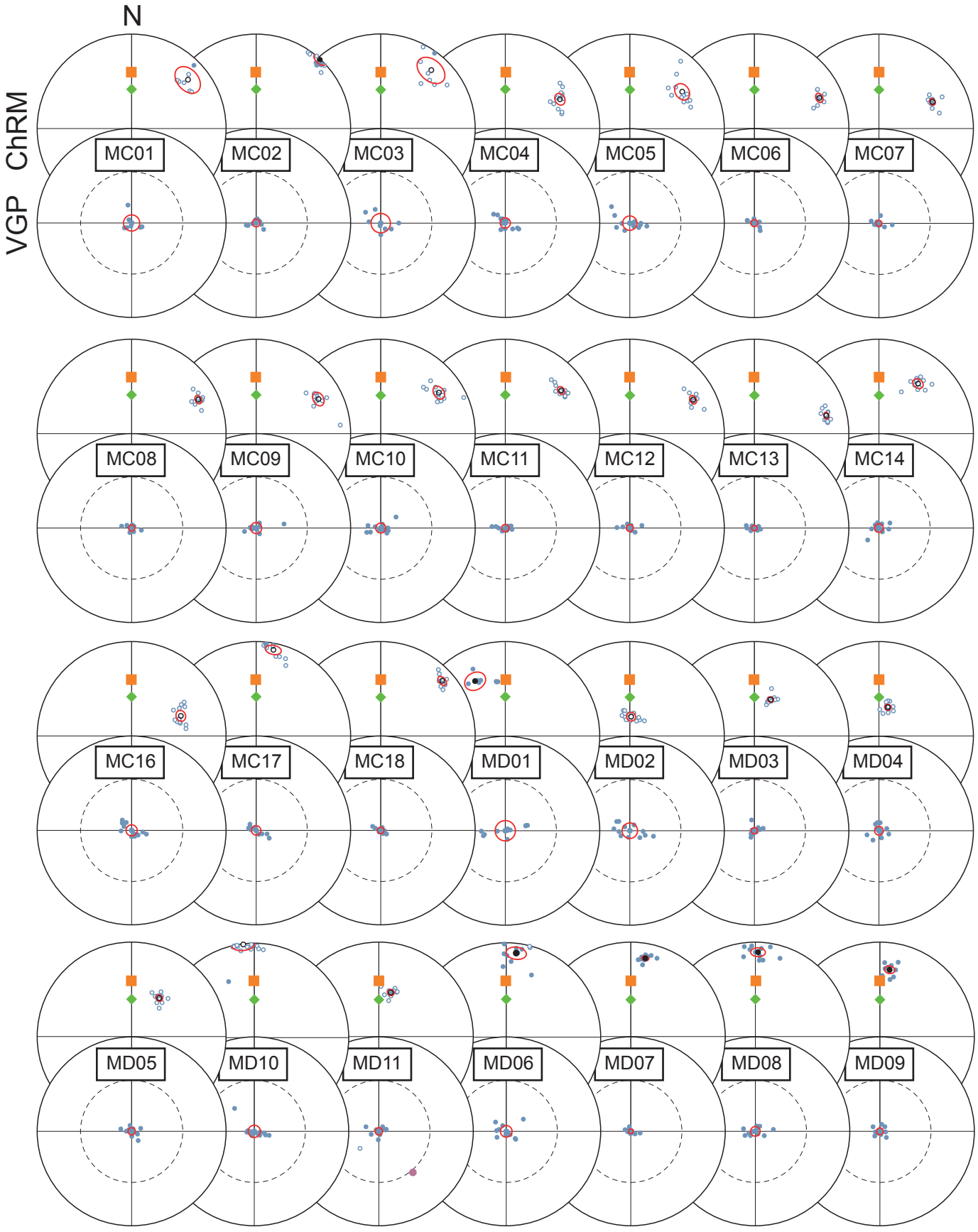
N
VGP ChRM
MC01
MC02
MC03
MC04
MC05
MC06
MC07
MC08
MC09
MC10
MC11
MC12
MC13
MC14
MC16
MC17
MC18
MD01
MD02
MD03
MD04
MD05
MD10
MD11
MD06
MD07
MD08
MD09

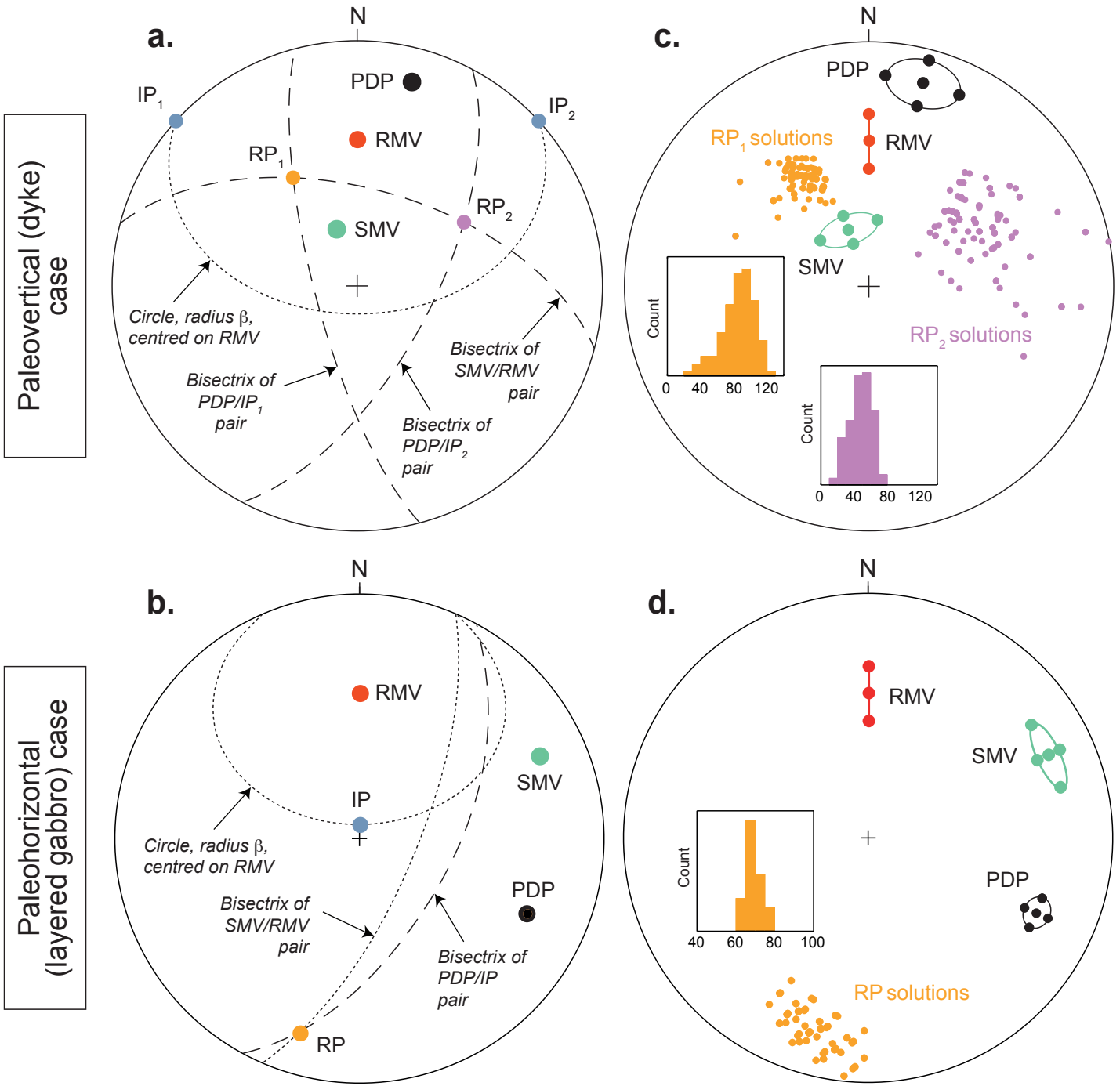
Paleovertical (dyke) case
a.
N
PDP
RMV
SMV
IP1
IP2
RP1
RP2
Circle, radius β, centred on RMV
Bisectrix of PDP/IP1 pair
Bisectrix of PDP/IP2 pair
Bisectrix of SMV/RMV pair
c.
N
PDP
RMV
RP1 solutions
SMV
RP2 solutions
Count
0 40 80 120
Count
0 40 80 120
Paleohorizontal (layered gabbro) case
b.
N
RMV
SMV
IP
PDP
Circle, radius β, centred on RMV
Bisectrix of SMV/RMV pair
Bisectrix of PDP/IP pair
RP
d.
N
RMV
SMV
PDP
Count
40 60 80 100
RP solutions

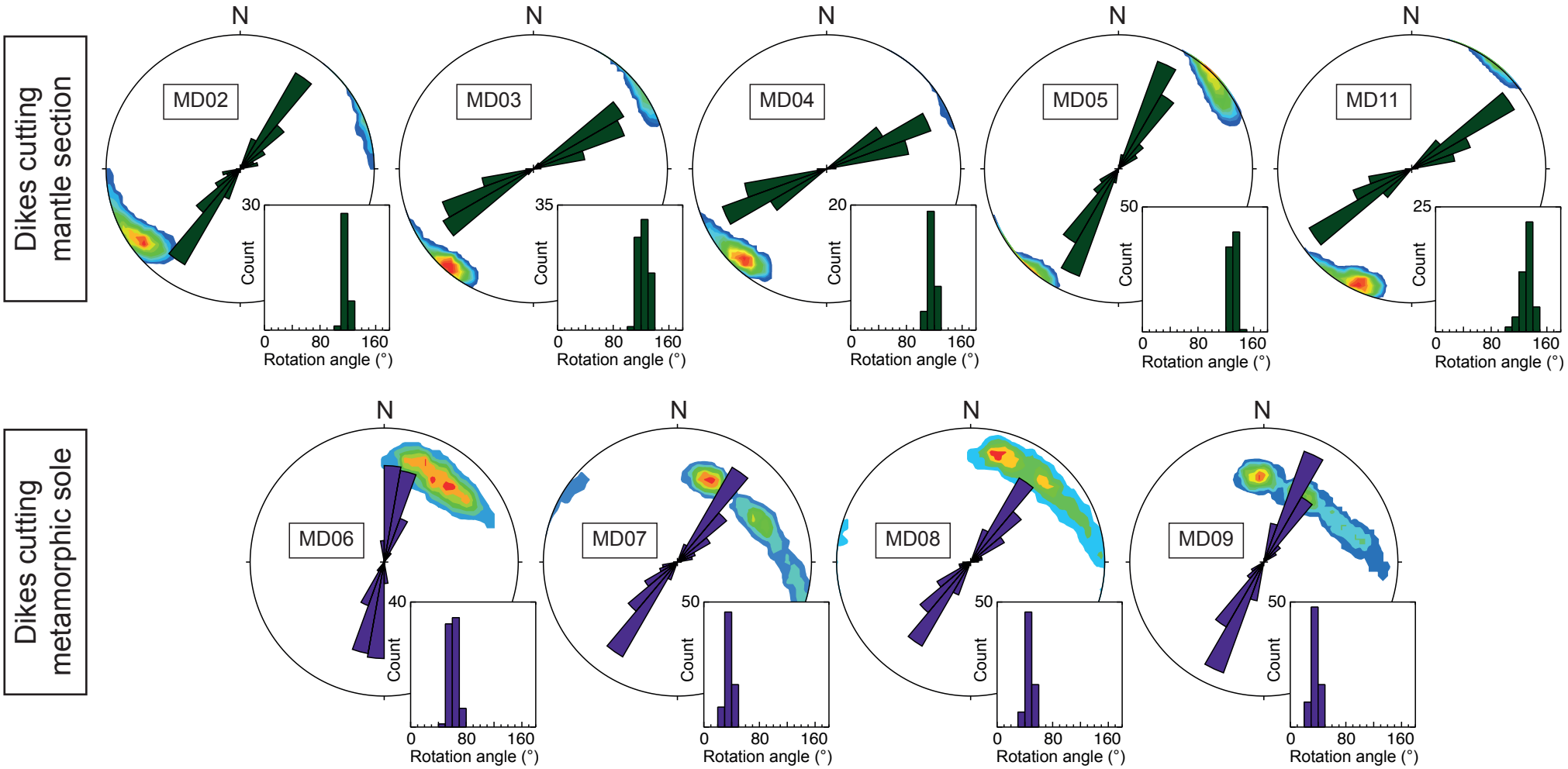
Dikes cutting mantle section
Dikes cutting metamorphic sole
N
MD02
MD03
MD04
MD05
MD11
MD06
MD07
MD08
MD09
Count
Rotation angle (°)
0
80
160
30
35
20
50
25
40

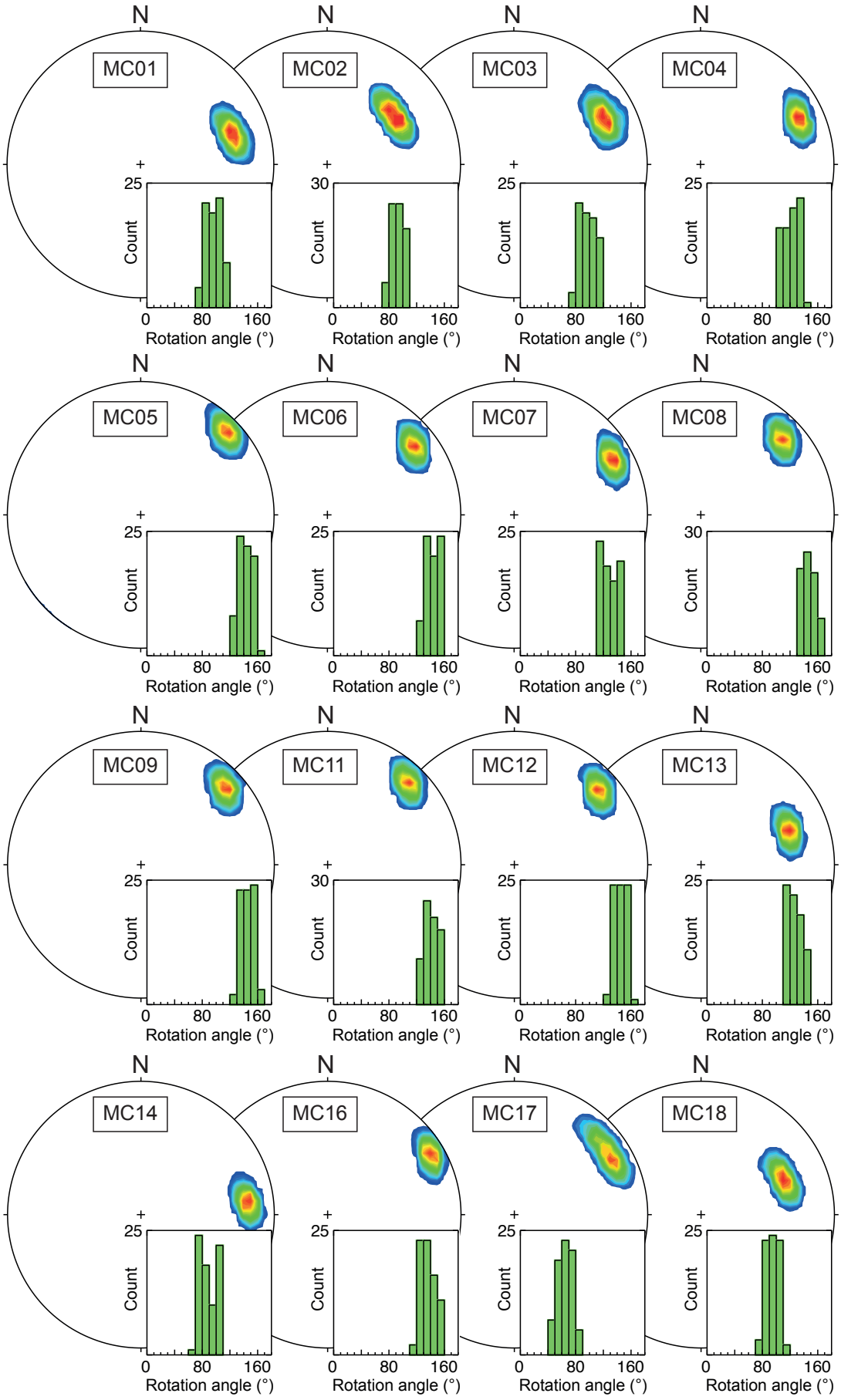
N
MC01
MC02
MC03
MC04
MC05
MC06
MC07
MC08
MC09
MC11
MC12
MC13
MC14
MC16
MC17
MC18
Count
Rotation angle (°)
0
80
160
25
30

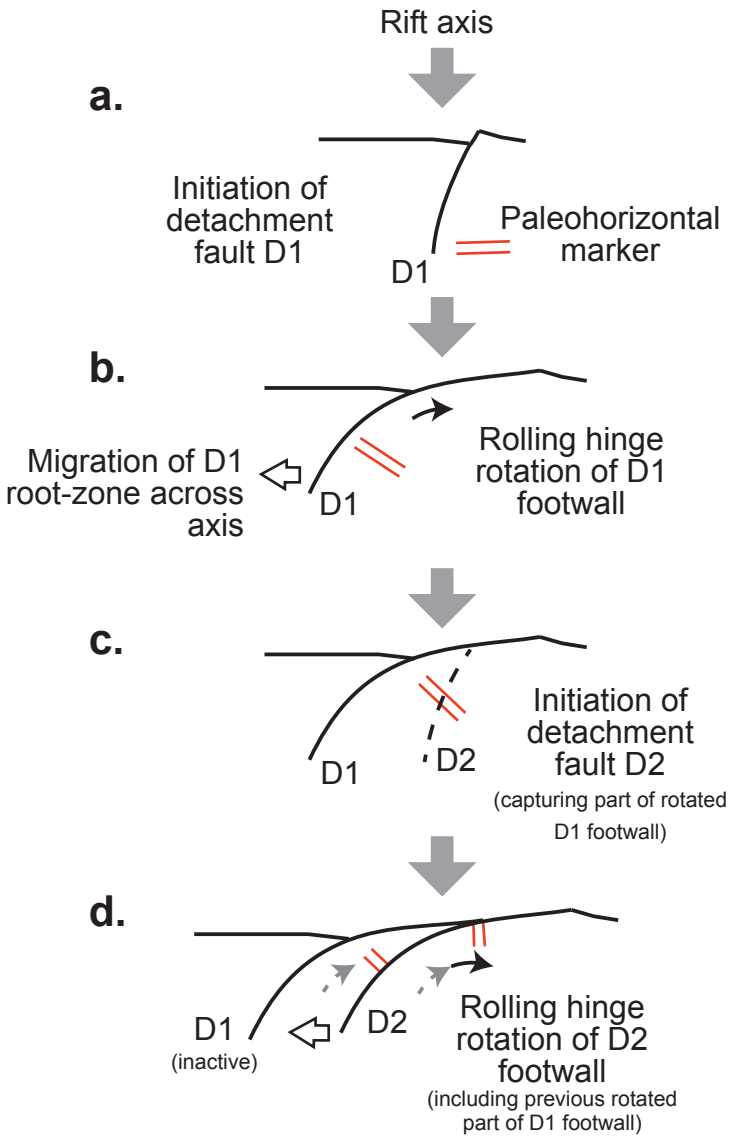
Rift axis
a.
Initiation of detachment fault D1
Paleohorizontal marker
D1
b.
Migration of D1 root-zone across axis
D1
Rolling hinge rotation of D1 footwall
c.
D1
D2
Initiation of detachment fault D2
(capturing part of rotated D1 footwall)
d.
D1
(inactive)
D2
Rolling hinge rotation of D2 footwall
(including previous rotated part of D1 footwall)